

Vibrations in an active controlled hexapod

Wouter Diederer

Date: March 2020
Thesis committee: Prof. Dr. ir. A. Metrikine,
Ir. V. Vaniushkina
Ir. J.J. Flohil
Ir. O. Kooy

TU Delft, Chairman
TU Delft, Supervisor
Ampelmann B.V.
Ampelmann B.V.



Acknowledgement

I would like to express my sincere gratitude to Prof. Andrei Metrikine, chairman of the graduation committee who gave me the opportunity to graduate under his supervision. The same applies for Valentina Vaniushkina, who performed the role of daily supervisor. This project has been made possible by Ampelmann. I would like to thank all the people from Ampelmann who helped me during my work. It was a pleasure working there. I especially would like to thank Jasper Flohil and Otto Kooy for their supervision and guidance. Without their support and input, I could not have completed this research successfully.

Abstract

Safe offshore access for people and cargo is a major challenge in the offshore industry. The Ampelmann system is an active motion compensated system for six degrees of freedom. Creating a platform isolated from the motions of the vessel making offshore access as easy as crossing the street. All the Ampelmann system can be used for people transfer, while some of the systems can also be used as a cargo crane. The basic system can be divided in two main systems: the hexapod and the transfer deck and gangway. Usually the system is installed on a ship deck. However, in various cases the height of the Ampelmann system is not sufficient to reach the landing point. An often-used solution is to place the system on a pedestal which can be over 15 meters high. The Ampelmann system occasionally starts vibrating unexpectedly, especially while the system is placed on a pedestal. These vibrations are believed to be caused by the eigenfrequencies of the system and/or amplification caused by the motion control algorithm. In this research an investigation in this phenomenon was done.

This investigation was done via an analysis of the eigenfrequencies of the active controlled hexapod. A finite element method model was created to determine the eigenfrequencies of the system. This model was made using MATLAB and the toolbox StaBIL 2.0, created by the university of Leuven. All the elements of the system are modeled as beams except the hydraulic actuators. The properties of the elements which represent the hydraulic actuators are calculated separately using a modelling study on stiffness characteristics of hydraulic cylinder under multi-factors.

Possible causes for the unexpected vibrations have been investigated via measurements performed on Ampelmann systems. Data which was readily available is analyzed. Based on this data three possible causes have been determined. These are: the influence of the pedestal, residual motions due to limitations of the Ampelmann system and vibrations in the bottom frame due to compensating for gangway motions.

To investigate the influence of the pedestal and the vibrations in the bottom frame two experiments have been performed. The residual motions have been investigated via calculations based on data already available. The amplitude of the response in the results from the first experiment performed to investigate the vibrations in the bottom frame due to gangway motions is negligible over the entire test period. The data from the calculations done to investigate the effect of the residual motions show no amplification. The results of the experiment and the calculations lead to the conclusion that these do not cause unwanted behavior.

The second experiment to determine the influence of the pedestal shows four peaks in the frequency domain of both the signals. The first is directly caused by vessel motions. The other three have a cause which is not directly related to vessel motions. The data from the sensor on the Ampelmann system, at the top of the pedestal, does not contain a peak which is not present at the ship deck. From this it can be concluded that the eigenfrequencies of the pedestal do not have a relevant influence. For one of these peaks the amplitude of the graph related to the top of the pedestal is higher than the one corresponding to the ship deck. A possible explanation for this phenomenon could be the eigenfrequencies and corresponding eigenmodes of the ship deck. The pedestal functions as a lever arm amplifying the rotations related to eigenmodes of the ship deck. This may cause the unexpected vibrations.

Ampelmann's motion control algorithm is complicated which makes it difficult to incorporate this algorithm in the FEM model. An attempt is made to create a simplified 2D multi-body model including the algorithm. At Ampelmann a model made by Temporary Work Design was available, consisting out of two masses, which should have functioned as the base for this model. During the investigation of the model an error was discovered. The correction of this error resulted in an unstable system. A pole plot investigation is done. However, no explanation for the instability is found.

Table of contents

1. INTRODUCTION	1
1.1 RESEARCH OBJECTIVE	3
1.2 THESIS OUTLINE	3
2. MOTION CONTROL ALGORITHM	4
2.1 CONTROL ENGINEERING	4
2.1.1 FEEDBACK	4
2.1.2 CONTROL	4
2.2 AMPELMANN'S MOTION CONTROL ALGORITHM	5
2.2.1 SIGNAL PROCESSING	5
2.2.2 INVERSE KINEMATICS	5
2.2.3 ACTUATORS CONTROLLER	6
3. EIGENFREQUENCIES AMPELMANN SYSTEM	8
3.1 BEAM ELEMENT	9
3.1.1 AXIAL STIFFNESS	9
3.1.2 BENDING MOMENTS	10
3.2 HYDRAULIC ACTUATOR	11
3.2.1 CYLINDER BARREL EXPANSION STIFFNESS	12
3.2.2 HYDRAULIC OIL STIFFNESS	12
3.3 FEM MODEL	13
3.3.1 A-TYPE	13
3.3.2 E-TYPE	15
3.4 CONCLUDING REMARKS	17
4. EXPERIMENTAL RESEARCH	18
4.1 EXPERIMENTAL FREQUENCY ANALYSIS	18
4.1.1 DISCRETE FOURIER TRANSFORM	18
4.1.2 SPECTRUM AVERAGING	19
4.1.3 FORWARD KINEMATICS OF A STEWART PLATFORM	20
4.2 PRE-PROCESSING	21
4.2.1 A-TYPE AND E-TYPE	21
4.3 POSSIBLE CAUSES OF UNEXPECTEDLY OCCURRING VIBRATIONS	25
4.3.1 INFLUENCE OF THE PEDESTAL	26
4.3.2 RESIDUAL MOTIONS	27
4.3.3 VIBRATIONS IN THE BOTTOM FRAME DUE TO COMPENSATING FOR GANGWAY MOTIONS	28

4.4	MEASUREMENTS ON THE AMPELMANN SYSTEM	29
4.4.1	INFLUENCE OF THE PEDESTAL	29
4.4.2	RESIDUAL MOTIONS	35
4.4.3	VIBRATIONS IN THE BOTTOM FRAME	37
4.5	CONCLUDING REMARKS	39
5.	<u>ANALYTICAL MODEL</u>	40
5.1	MODEL BY TEMPORARY WORK DESIGN	40
5.2	DIFFERENTIATION ERROR	42
5.3	POLE PLOT INVESTIGATION	43
5.4	CONCLUDING REMARKS	44
6.	<u>CONCLUSION AND RECOMMENDATIONS</u>	45
6.1	CONCLUSION	45
6.2	RECOMMENDATIONS	46
7.	<u>REFERENCES</u>	47
8.	<u>APPENDIX</u>	49

List of figures

FIGURE 1-1: AMPELMANN SYSTEM	1
FIGURE 1-2: SIMPLIFIED CONTROL LOOP	1
FIGURE 1-3: GENERIC A FRAME	2
FIGURE 2-1: CLOSED LOOP (LEFT); OPEN LOOP (RIGHT)	4
FIGURE 2-2: BOTTOM AND TOP FRAME COORDINATE SYSTEM	6
FIGURE 2-3: AMPELMANN'S MOTION CONTROL ALGORITHM.....	7
FIGURE 3-1: HEXAPOD, TRANSFER DECK AND GANGWAY (NODES AND ELEMENTS).....	8
FIGURE 3-2: BEAM ELEMENT	9
FIGURE 3-3: AXIAL STIFFNESS BEAM ELEMENT.....	10
FIGURE 3-4: BENDING STIFFNESS BEAM ELEMENT	10
FIGURE 3-5: HYDRAULIC ACTUATOR.....	11
FIGURE 3-6: HYDRAULIC SYSTEM [7]; 1 CYLINDER BARREL, 2 HYDRAULIC OIL, 3 PISTON SEALING, 4 ROD SEALING, 5 PISTON ROD, 6 FLEXIBLE HOSE, 7 METAL PIPE	11
FIGURE 3-7: FEM MODEL A-TYPE SYSTEM	13
FIGURE 3-8: MODE SHAPES 1 TO 4 A-TYPE SYSTEM	14
FIGURE 3-9: FEM MODEL E-TYPE SYSTEM.....	15
FIGURE 3-10: MODE SHAPES 1 TO 4 E-TYPE SYSTEM.....	16
FIGURE 4-1: SUMMARY OF DISCRETE FOURIER TRANSFORM [11].....	19
FIGURE 4-2: SEGMENT-BASED FREQUENCY DOMAIN AVERAGING [12]	20
FIGURE 4-3: LOCATION OF THE MOTION SENSORS	22
FIGURE 4-4: TRANSLATIONS A-TYPE SYSTEMS	22
FIGURE 4-5: ROTATIONS A-TYPE SYSTEMS.....	23
FIGURE 4-6: DIFFERENCE BETWEEN MRU 1 AND MRU 2 IN HEAVE DIRECTION FOR A-TYPE SYSTEMS	23
FIGURE 4-7: TRANSLATIONS E-TYPE SYSTEMS.....	24
FIGURE 4-8: ROTATIONS E-TYPE SYSTEMS	24
FIGURE 4-9: DIFFERENCE BETWEEN MRU 1 AND MRU 2 IN HEAVE DIRECTION FOR E-TYPE SYSTEMS	25
FIGURE 4-10: OVERVIEW AMPELMANN SYSTEM.....	25
FIGURE 4-11: CROSS SECTION OF AMPELMANN SYSTEM; VIBRATIONS CAUSED BY A PEDESTAL	26
FIGURE 4-12: CROSS SECTION OF AMPELMANN SYSTEM; RESIDUAL MOTIONS	27
FIGURE 4-13: CROSS SECTION OF AMPELMANN SYSTEM; VIBRATIONS IN THE BOTTOM FRAME	28
FIGURE 4-14: MRU LOCATIONS.....	30
FIGURE 4-15: SHIP TO SHIP MRU	30
FIGURE 4-16: LEAVER ARMS (DX & DZ).....	31
FIGURE 4-17: E-04 TRANSLATIONS (TIME DOMAIN)	32
FIGURE 4-18: E-04 ROTATIONS (TIME DOMAIN)	32
FIGURE 4-19: E-04 TRANSLATIONS (FREQUENCY DOMAIN).....	33
FIGURE 4-20: E-04 ROTATIONS (FREQUENCY DOMAIN).....	33
FIGURE 4-21: SCHEMATIC OVERVIEW SHIP DECK VIBRATIONS	34
FIGURE 4-22: CYLINDER LENGTHS AND REFERENCE MOTIONS	35
FIGURE 4-23: RESIDUAL MOTIONS (TIME AND FREQUENCY DOMAIN).....	36
FIGURE 4-24: OVERVIEW EXPERIMENT VIBRATIONS IN THE BOTTOM FRAME.....	37
FIGURE 4-25: A-20 TRANSLATIONS AND ROTATIONS (ENTIRE SAMPLED TIME).....	38
FIGURE 4-26: A-20 TRANSLATIONS AND ROTATIONS (SAMPLED TIME SERIES DURING SINGLE BLOW WITH GANGWAY).....	38
FIGURE 5-1: OVERVIEW OF DESIRED RESULT	40
FIGURE 5-2: TWD MODEL [15].....	41
FIGURE 5-3: INTRODUCTION OF CYLINDER MODEL [15]	41

FIGURE 5-4: CONTROL LOOP IN ANALYTICAL MODEL	42
FIGURE 5-5: POLE-ZERO MAP OF CLOSED LOOP, LEFT WITH ERROR & RIGHT WITHOUT ERROR	43
FIGURE 5-6: POLE ZERO MAPS; LEFT: PLANT, RIGHT: CONTROLLER	44
FIGURE 5-7: POLE ZERO MAPS; LEFT: LOWPASS FILTER FEED FORWARD, RIGHT: OPEN LOOP	44
FIGURE 8-1: STANDARD BLOCK DIAGRAM ELEMENTS [2]	49
FIGURE 8-2: TIME DOMAIN A-28 SYSTEM	51
FIGURE 8-3: TIME DOMAIN A-29 SYSTEM	51
FIGURE 8-4: TIME DOMAIN E-04 SYSTEM	52
FIGURE 8-5: TIME DOMAIN E-14 SYSTEM	52
FIGURE 8-6: A-28 WITHOUT PEDESTAL (UPPER), A-29 WITH PEDESTAL (LOWER).....	53
FIGURE 8-7: E-04 ON PEDESTAL (UPPER), OLYMPIC ORION, NO PICTURE WITH AMPELMANN SYSTEM AVAILABLE (LOWER)	53
FIGURE 8-8: MRU (OCTANS) SPECIFICATIONS	54
FIGURE 8-9: E-04 TRANSLATIONS DIFFERENCE (TIME DOMAIN)	55
FIGURE 8-10: E-04 ROTATIONS DIFFERENCE (TIME DOMAIN)	55
FIGURE 8-11: E-04 TRANSLATIONS DIFFERENCE (FREQUENCY DOMAIN)	56
FIGURE 8-12: E-04 ROTATIONS DIFFERENCE (FREQUENCY DOMAIN)	56
FIGURE 8-13: RESPONSE ANALYTICAL MODEL	57

1. Introduction

Safe offshore access for people and cargo is a major challenge in the offshore industry. The Ampelmann system is an active motion compensated system for six degrees of freedom. Creating a platform isolated from the motions of the vessel making offshore access as easy as crossing the street. All the Ampelmann system can be used for people transfer, while some of the systems can also be used as a cargo crane. The basic system can be divided in two main systems: the hexapod and the transfer deck and gangway (Figure 1-1, left). Usually the system is installed on a ship deck. However, in various cases the height of the Ampelmann system is not sufficient to reach the landing point. An often-used solution is to place the system on a pedestal which can be over 15 meters high (Figure 1-1, right).

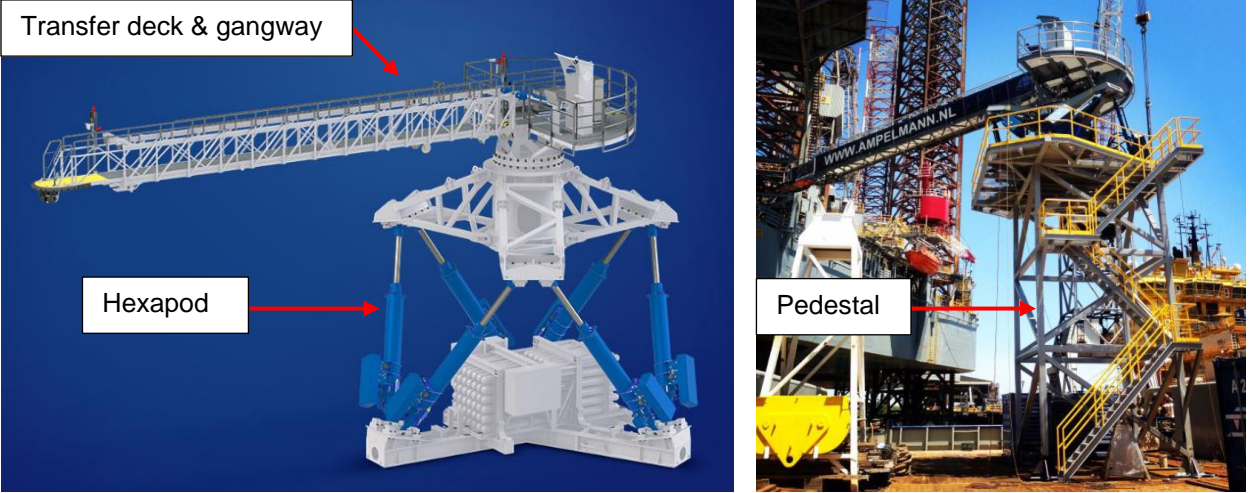


Figure 1-1: Ampelmann system

Hexapod

The hexapod is based on a Stewart platform [1] consisting of a bottom frame, a base frame and six hydraulic cylinders. The bottom frame is fixed to the vessel or pedestal. The transfer deck is connected to the base frame. The hexapod or Stewart platform is the system that compensates the vessel motions. The control of the hexapod is based on the displacement and velocity measured by sensors located at the base frame of the system. A simplified model of the control loop is given in Figure 1-2. In this figure $X_{ref,global}$ and $X_{ref,measured}$ are the desired and measured location of the transfer deck and gangway and L_{cyl} is the length of the cylinders.

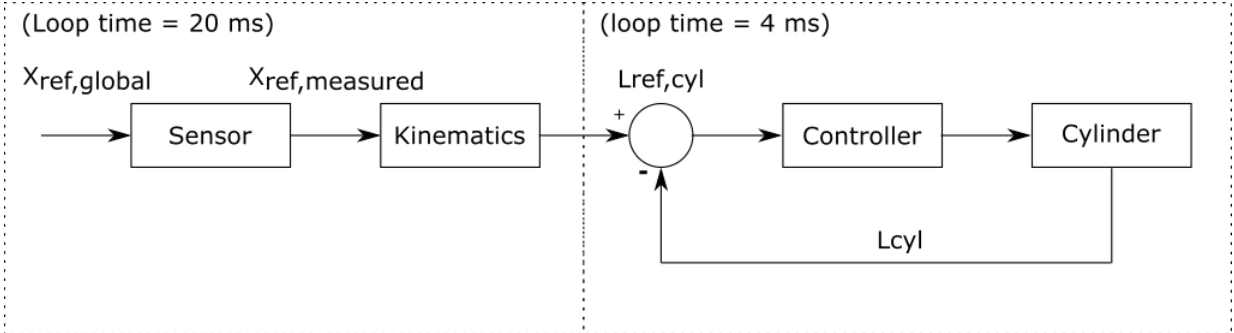


Figure 1-2: Simplified control loop

Transfer deck & gangway

Personnel accessing an offshore structure from a ship via an Ampelmann system commence their crossing on the transfer deck. The system starts up after which the people transfer begins. Personnel walk over the gangway to the offshore structure. The gangway can maneuver in three degrees of freedom, basically resembling the boom of a crane.

Pedestal

The pedestals, which are used by Ampelmann to increase the possible height of the landing point, are mostly individually designed. At the moment, Ampelmann is in the process of designing a generic A-frame (GAF). This will be a modular based pedestal (Figure 1-3).

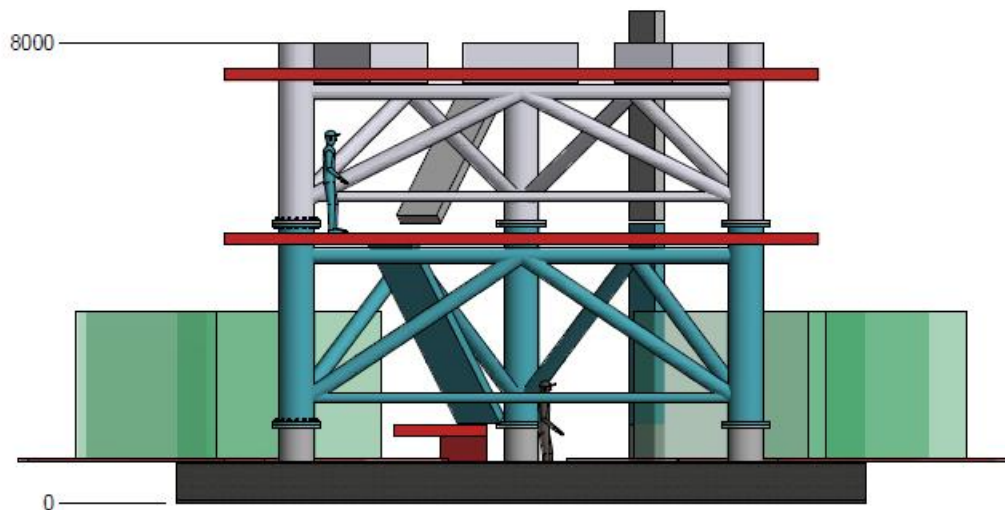


Figure 1-3: Generic A frame

A-type & E-type

Ampelmann employs three types of systems. The A-type, E-type and L-type. The L-type does not use a hexapod so no investigation regarding this type will be done in this research. The A-type is an offshore access system for performing safe transfer of personnel in sea states with a maximum significant wave height of 3 meters. The system weights roughly 40 tons and has a gangway length of 20 to 25 meters. The E-type is designed to safely transfer offshore personnel in rough sea conditions. The gangway system is based on the same technology as the A-type, only 1.5 times larger. As a result of its increased size, the E-type is capable of compensating sea states up to 4.5 meters significant wave height. The systems weights roughly 100 tons and has a gangway length of 25 to 30 meters.

1.1 Research objective

The Ampelmann system occasionally starts vibrating unexpectedly, especially while the system is placed on a pedestal. These vibrations are believed to be caused by the eigenfrequencies of the system and/or amplification caused by the motion control algorithm. At the moment, the knowledge present at Ampelmann about these vibrations is mostly based on field experience. In this research an investigation in this phenomenon will be done. To perform this the following research goal is formulated:

The objective of this thesis is performing an analysis on the eigenfrequencies of an active controlled hexapod and explain the unexpectedly occurring vibrations in the Ampelmann system.

To reach the research goal a set of sub goals are formulated:

1. *Design a model which can be used to calculate the eigenfrequencies and corresponding eigenmodes of an Ampelmann system.*
2. *Investigate whether motion compensation caused by vibrating of the pedestal can cause the unexpected vibrations in an Ampelmann system.*
3. *Determine the frequency content of the residual motions and compare them to the eigenfrequencies of the gangway which might cause the unexpectedly occurring vibrations in an Ampelmann system.*
4. *Investigate whether vibrations in the bottom frame, due to compensating for gangway motions, can cause the unexpected vibrations in an Ampelmann system*
5. *Create a simplified multibody model incorporating the motion control algorithm which can explain the unexpectedly occurring vibrations in an Ampelmann system.*

The first sub goal, about the eigenfrequencies of the system, helps to reach the first part of the research goal. The second, third and fourth aim to answer the second part of the research goal. These come down to investigating whatever happens below the hexapod, what happens due to limitations of the hexapod and what happens above the hexapod. The fifth sub goal aims to combine all the data into a single model and explain the vibrations.

1.2 Thesis outline

This thesis consists out of a total of six chapters. The first step in this work is a brief discussion about control engineering and the motion control algorithm used by Ampelmann in chapter 2. Next, in chapter 3, a finite element method model is created to determine the eigenfrequencies of the system and sub-systems. In chapter 4 some experimental research is done to identify and explain possible causes for the unexpectedly occurring vibrations. In chapter 5 a simplified 2D multi-body model is created. However, due to an error, which will be explained later, in a template model which was supposed to be used, a small research regarding this mistake is done. Chapter 6 summarizes the conclusions of this research and adds recommendations.

2. Motion control algorithm

The Ampelmann motion control algorithm (Figure 2-3) calculates and controls the required lengths of the hydraulic actuators such that the transfer deck experiences no rotations and translations. The goal of this chapter is to get a basic understanding of motion control engineering and Ampelmann's algorithm. First some general motion control engineering theory is given. Next the control algorithm is discussed. The algorithm consists of three parts: Signal processing, kinematics and the controller. These three parts will be discussed briefly.

2.1 Control engineering

Motion control engineering focuses on moving a load from one place to another by precisely controlling the position, velocity and the acceleration of the load under defined operating conditions. The basic principles of motion control can be divided in feedback and control. Feedback refers to the situation where two or more dynamic systems are connected and influence each other's behavior over time. Control is the design of component of an engineering feedback system to achieve a desired behavior [2].

2.1.1 Feedback

A dynamical system is a system whose behavior changes over time. Feedback is about two or more connected dynamic systems such that they influence each other's behavior and are thus strongly coupled. Simple causal reasoning about a feedback system is difficult because the first system influences the second and vice versa. A consequence of this is that the behavior of a feedback system is often counterintuitive. This makes it necessary to investigate the entire system. Two often used terms when referring to such systems are open loop and closed loop systems (Figure 2-1). A system is closed loop when the systems are connected in a circle and open loop when this circle is broken. Feedback has potential disadvantages: It can create dynamic instabilities or even runaway behavior. A second drawback is that feedback can introduce unwanted sensor noise into a system requiring careful signal processing and filtering of the sensor signal [2].

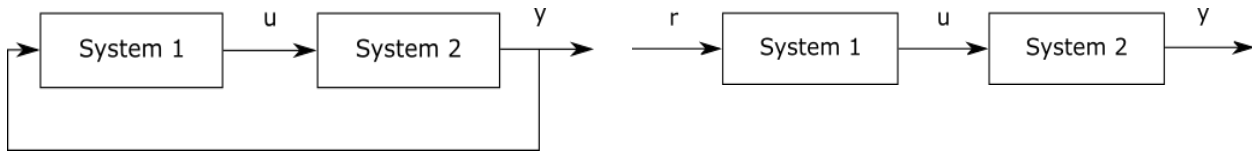


Figure 2-1: Closed loop (left); Open loop (right)

2.1.2 Control

In the area of motion control engineering the term control is defined as the use of algorithms and feedback in engineering systems. A modern controller senses the operation of a system, compares it to a desired behavior ($e = r - y$), and then computes corrective actions based on a model of the system's response to external inputs and actuates the system for a desired change. This loop of sensing, computation and actuation is a central concept in control engineering [2].

Proportional Integral Derivative control

Using only an on-off control often causes oscillations because the system overreacts. A small error causes a "full throttle" response in the system. This effect is avoided using proportional controller. The characteristic of the controller is proportional to a control error for small errors (equation 2.1). In this equation k_p is the controller gain and $e_{min} = u_{min}/k_p$ and $e_{max} = u_{max}/k_p$ is the proportional band where the behavior of the controller is linear.

$$u = \begin{cases} u_{max} & \text{if } e \geq e_{max} \\ k_p e & \text{if } e_{min} < e < e_{max} \\ u_{min} & \text{if } e \leq e_{min} \end{cases} \quad (2.1)$$

A proportional controller is a huge improvement compared to an on-off controller. However, a proportional controller has the drawback that some level of control signal is required for the system to maintain a desired value, meaning $e \neq 0$. This can be avoided by making the control action proportional to the integral of the error (equation 2.2), which is called an integral controller. This controller has zero steady state error [2]. The problem however is that there may not always be a steady state because the system is for example oscillating.

$$u(t) = k_i \int_0^t e(\tau) d\tau \quad (2.2)$$

An additional refinement is to provide the controller with a predictive ability by using a prediction of the error. The simplest form is using a linear extrapolation (equation 2.3) predicting the error T_d units of time ahead.

$$e(t + T_d) = e(t) + T_d \frac{de(t)}{dt} \quad (2.3)$$

Combining these three actions, proportional, integral and derivative control results in a PID controller which is mathematically expressed in equation 2.4.

$$u(t) = k_p e(t) + k_i \int_0^t e(\tau) d\tau + k_d \frac{de(t)}{dt} \quad (2.2)$$

2.2 Ampelmann's motion control algorithm

The orientation of the bottom frame is acquired from a 6 degree of freedom motion sensor located at the center of the bottom frame. Using this data, the necessary lengths of the hydraulic actuators are calculated using inverse kinematics. These lengths are sent to a controller which controls the length of the cylinder using a feed forward and multiple feedback loops.

2.2.1 Signal processing

The sensors measure, in 6 degrees of freedom, the motions of the vessel. These contain a high frequency part for which the Ampelmann system should not compensate. This part of the signal is filtered using a low pass filter. The S-curve is used to slowly start up the system. Instead of going to full compensation instantly, the process is smoothed over a period of time. The main goal of this part of the motion control algorithm is creating a signal in which all unwanted parts are removed resulting in a clean signal which can be used for motion compensating.

2.2.2 Inverse kinematics

The pose of a Stewart platform can be defined by the position and orientation of the top and bottom frame with respect to each other [3]. The lengths of the 6 actuators can be determined with these orientations using inverse kinematics. The orientation of the bottom frame is measured by a six degree of freedom motion sensor. This sensor is located at the center of the bottom frame while the top frame is assumed to be horizontal and motionless. Two local coordinate systems (Figure 2-2) are introduced one at center of the top frame (O_t) and one at the center of the bottom frame (O_b). The coordinates of the bottom joints are expressed in the coordinates system of the top frame using a rotation matrix. The required lengths of the hydraulic actuators can now be determined.

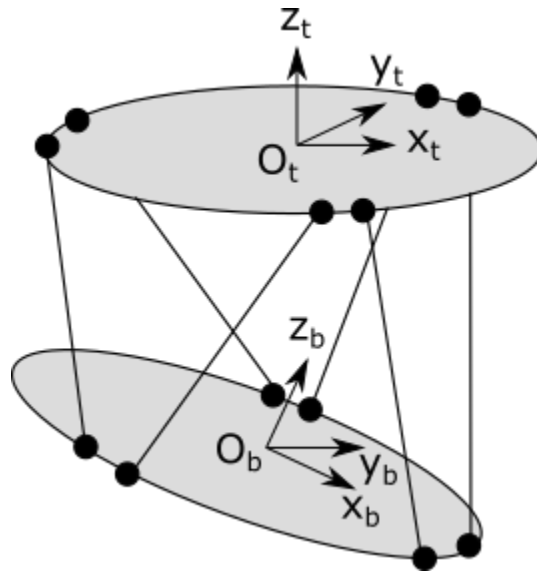


Figure 2-2: Bottom and top frame coordinate system

2.2.3 Actuators controller

The Ampelmann controller is relatively complicated, consisting out of a saturation block, rate limiter, lookup tables, S-curves etcetera. For details see appendix A. However, the general idea of the controller is the following: The input of the controller is the error between the reference lengths and the actual lengths of the actuators and the error between the reference velocity and actual velocity of the actuator. These errors are translated into a certain pressure. This pressure results in the output. The output is the valve position in the hydraulic actuators.

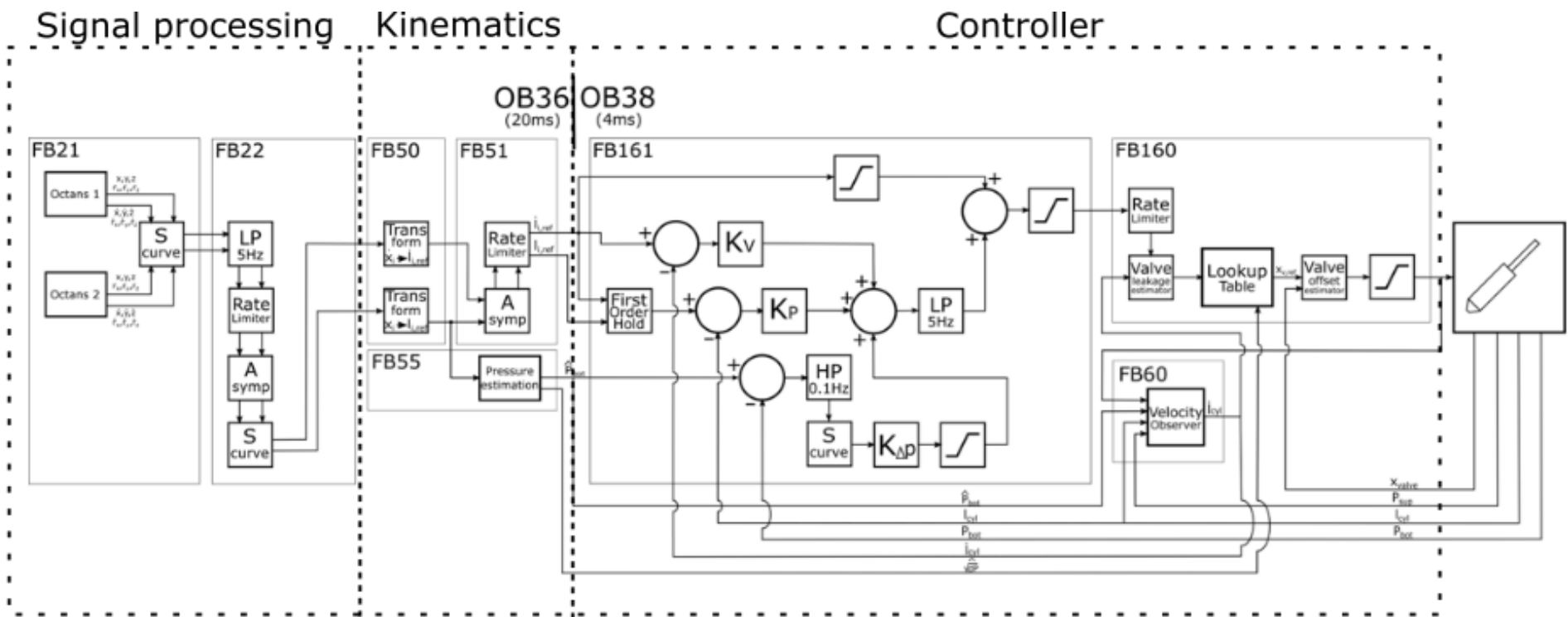


Figure 2-3: Ampelmann's motion control algorithm

3. Eigenfrequencies Ampelmann system

To mimic the unexpectedly occurring vibrations, two computer models are made. The first model will be used to determine the eigenfrequencies of the system. This model is made using MATLAB and the toolbox StaBIL 2.0 [4], created by the university of Leuven resulting in a finite element method model. The finite element method model will be used to determine eigenfrequencies and eigenmodes. The FEM model is created using the toolbox StaBIL 2.0. The toolbox consists out of a set of MATLAB functions which perform a matrix method based discrete-element idealization. StaBIL 2.0 is based on [5] & [6].

A discrete-element model of the Ampelmann system will be created. In Figure 3-1 an example of the hexapod, transfer deck and gangway is given. The system is assumed to exist out of a set of beams coupled by rigidly connected joints. The interaction forces between the various elements are represented by joint forces. These joint forces are axial forces, shear forces, bending moments and torques. For each element a local stiffness and mass matrix is composed which will be transferred to the global coordinates system using a matrix. For elements which are long compared to their cross section dimension the elastic characteristics can be determined accurately [5]. The pedestal and transfer deck and gangway are all assembled using beam elements. The hexapod is also assembled using beam elements. However, the stiffness and mass of elements which represent the hydraulic actuators are calculated separately using a modelling study on stiffness characteristics of hydraulic cylinder under multi-factors [7].

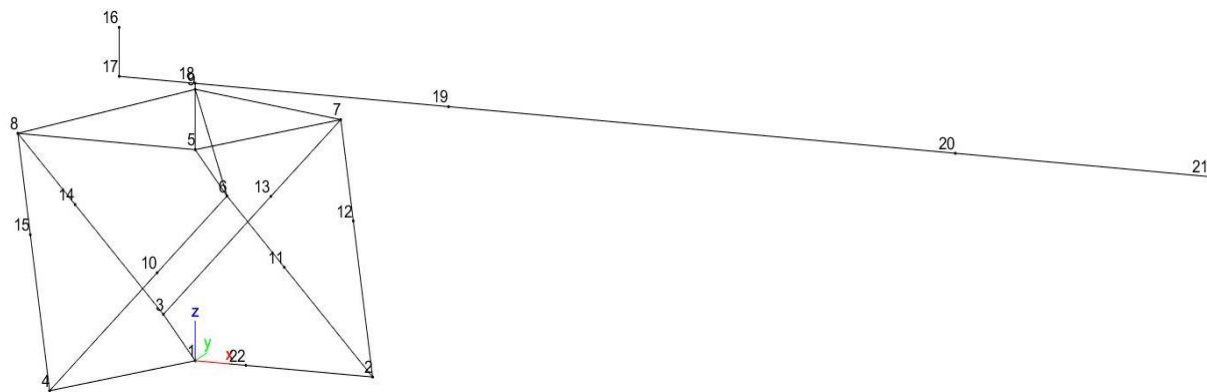


Figure 3-1: Hexapod, transfer deck and gangway (nodes and elements)

3.1 Beam element

Beam elements are assumed to be straight members of uniform cross section capable of resisting axial forces, bending moments about its two principal axes in plane of its cross section and a twisting moment about its centroidal axis. The location and positive direction of the degrees of freedom are given in Figure 3-2. The position of the beam element in space is specified by the location of the p-end of the beam and the direction of the local x-axis. The stiffness and mass matrix for a uniform beam element are derived directly from the differential equations for beam displacements in engineering beam theory [5] & [6]. The entire stiffness matrix is given in appendix B. The two most dominant stiffness properties, axial and bending, are worked out below. For the other stiffness parameters reference is made to [5].

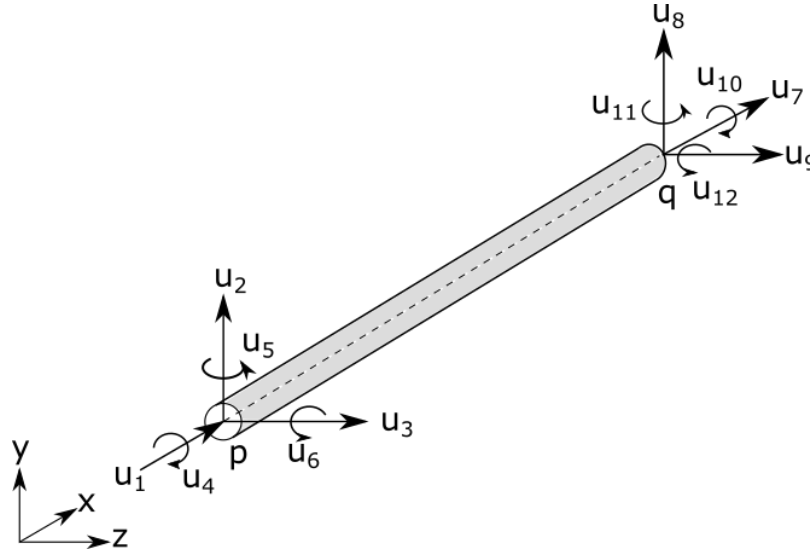


Figure 3-2: Beam element

3.1.1 Axial stiffness

The differential equation for axial displacement is:

$$F_1 = -\frac{du_1}{dx}EA \quad (3.1)$$

This equation can be integrated and by assuming the following boundary conditions: The left end of the beam at $x = 0$ has a displacement u_1 and the right end at $x = l$ has zero displacement (Figure 3-3). This results in the following solution:

$$F_1 = \frac{EA}{l}u_1 \quad (3.2)$$

From equation 3.2 and force equilibrium in the x direction, the axial stiffnesses can be computed:

$$k_{1,1} = -k_{7,1} = k_{7,7} = \frac{EA}{l} \quad (3.3)$$

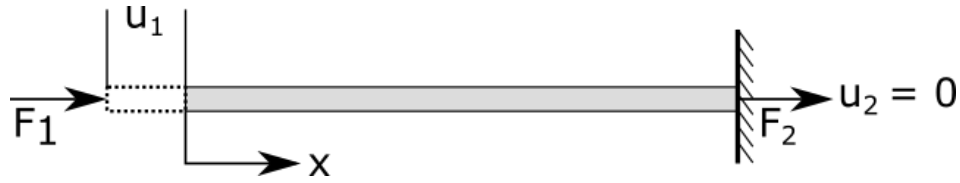


Figure 3-3: Axial stiffness beam element

3.1.2 Bending moments

The differential equation for deflection of the beam is:

$$EI_z \frac{d^2 u_2}{dx^2} = F_2 x - F_6 \quad (3.4)$$

The following boundary conditions are assumed:

$$\begin{aligned} u_2 = u_8 = 0 \\ \frac{du_8}{dx} = -\frac{F_2}{GA_s} \quad \text{at } x = l \end{aligned} \quad (3.5)$$

Equation 3.4 can be integrated and by applying the boundary conditions, equilibrium and symmetry, the bending stiffness can be determined:

$$\begin{aligned} k_{6,6} = k_{12,12} &= \frac{(4 + \phi)EI_z}{(1 + \phi)l} \\ \phi &= \frac{12EI}{GA_s l^2} \end{aligned} \quad (3.6)$$

The bending stiffness in the direction of u_5 and u_{11} can be determined in a similar way. Using the moment of inertia (I) and the effective shear area (A_s) with respect to the y -axis.

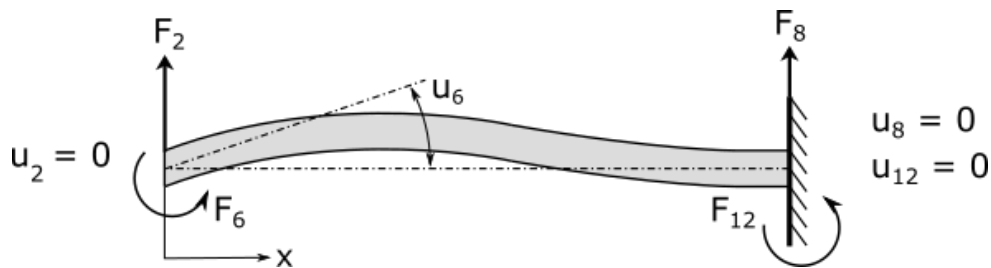


Figure 3-4: Bending stiffness beam element

3.2 Hydraulic actuator

Each hydraulic actuator is assumed to exist out of two elements (Figure 3-5). One represents the cylinder and one represents the piston. For all the degrees of freedom except the axial directions both the cylinder and the piston are modeled using the beam theory as explained in paragraph 3.1. However, the axial stiffness of a hydraulic actuator is significantly affected by the characteristics of, for example the bulk modulus of the hydraulic oil. The determination of the axial hydraulic actuator stiffness is based on [7].

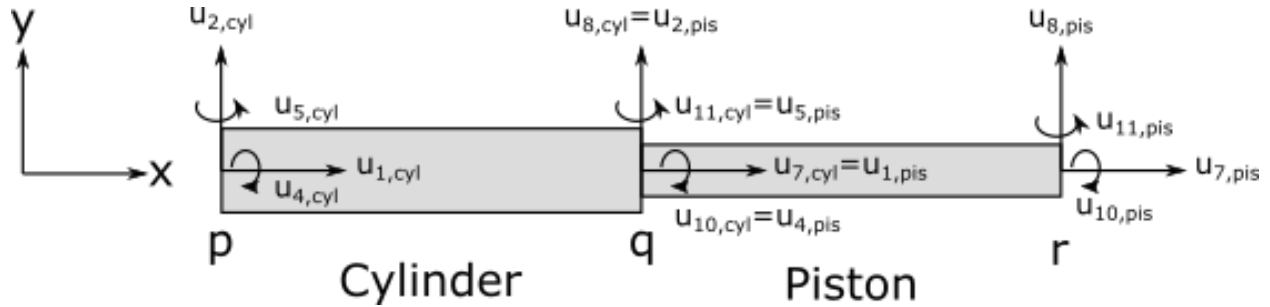


Figure 3-5: Hydraulic actuator

The main factors affecting the hydraulic actuator stiffness (Figure 3-6) are the hydraulic oil stiffness $[K_o]$, the piston rod axial stiffness $[K_r]$, the cylinder barrel expansion stiffness $[K_p]$, the flexible hose expansion stiffness $[K_h]$ and the sealing ring deformation stiffness $[K_s]$. The total stiffness can be determined as the sum of the reciprocals of the all the stiffnesses [7]. The level of influence of each stiffness according to [7] is: the hydraulic oil stiffness is about 80 %, the expansion deformation of the cylinder barrel is about 10 % and the axial deformation of the piston rod is about 6 % of the total. The other factors are smaller than 3 % and are neglected because of their small contribution. The cylinder actuator stiffness can be calculated using equation 3.7. The piston rod in general is a solid cylindrical steel rod. The axial stiffness is calculated based on beam theory, as given in paragraph 3.1.

$$\frac{1}{K} = \frac{1}{K_o} + \frac{1}{K_r} + \frac{1}{K_c} \quad (3.7)$$

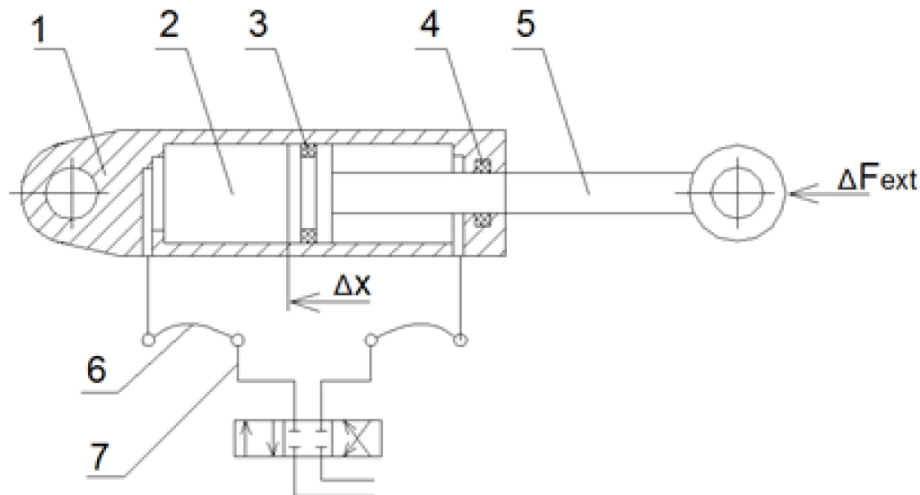


Figure 3-6: Hydraulic system [7]; 1 cylinder barrel, 2 hydraulic oil, 3 piston sealing, 4 rod sealing, 5 piston rod, 6 flexible hose, 7 metal pipe

3.2.1 Cylinder barrel expansion stiffness

The cylinder barrel expansion stiffness is produced by the movement of the piston as a result of the radial cylinder expansion caused by a pressure change $[\Delta P]$. The radial deformation $[\Delta D]$ due to a pressure change can be computed using equation 3.8, with D_o as the outer barrel diameter D_i as the inner barrel diameter, E_b is Young's modulus and ν_b as the Poisson ratio.

$$\Delta D = \frac{D\Delta P}{E_b} \left(\frac{D_o^2 + D_i^2}{D_o^2 - D_i^2} + \nu_b \right) \quad ; \quad \lambda_c = \frac{D_o^2 + D_i^2}{D_o^2 - D_i^2} \quad (3.8)$$

By calculating the volumetric change as a result of the radial deformation caused by the pressure change and using the spring stiffness equation $K_{sp} = df/dx$, the cylinder barrel expansion stiffness is given by equation 3.9. In this equation A is the cross section of the cylinder, L is the length of the cylinder and V is the volume of the cylinder.

$$K_c = \frac{\Delta P A^2}{\Delta V} = \frac{E_b A}{2L} * \frac{1}{\lambda_c + \nu_b} \quad (3.9)$$

3.2.2 Hydraulic oil stiffness

The hydraulic oil stiffness can be computed using the following equations:

$$K_o = E_o \frac{A^2}{V} \quad (3.10)$$

The oil bulk modulus $[E_o]$ is influenced by the amount of air in the fluid and the pressure of the fluid. The oil bulk modulus can be described using equation 3.11 [8]. In this equation, E_o' is the oil bulk modulus without air, p_a is the atmospheric pressure, α is the relative air content in oil under atmospheric pressure and n is the isentropic coefficient ($n = 1.4$).

$$E_o = E_o' \frac{1 + \alpha \left(\frac{p_a}{p_a + p} \right)^{1/n}}{1 + \alpha E_o' \frac{p_a^{1/n}}{n(p_a + p)^{(n+1)/n}}} \quad (3.11)$$

3.3 FEM model

3.3.1 A-type

In Figure 3-7 the FEM model of the A-type on a pedestal is plotted. The pedestal consists out of two GAF modules. To get some confidence the mass of the model is calculated and compared to masses from real systems. The mass is calculated using the volumes and densities of the elements. This results in a difference of less than 10 % for the A-type system when compared to the actual system, which is heavier. The object only contains structural members. The difference of 10 % can be explained by some miscellaneous like pipework and a stairway. In Figure 3-8 the first four eigenmodes of the system according are plotted and in Table 3-1 the corresponding eigenfrequencies are given.

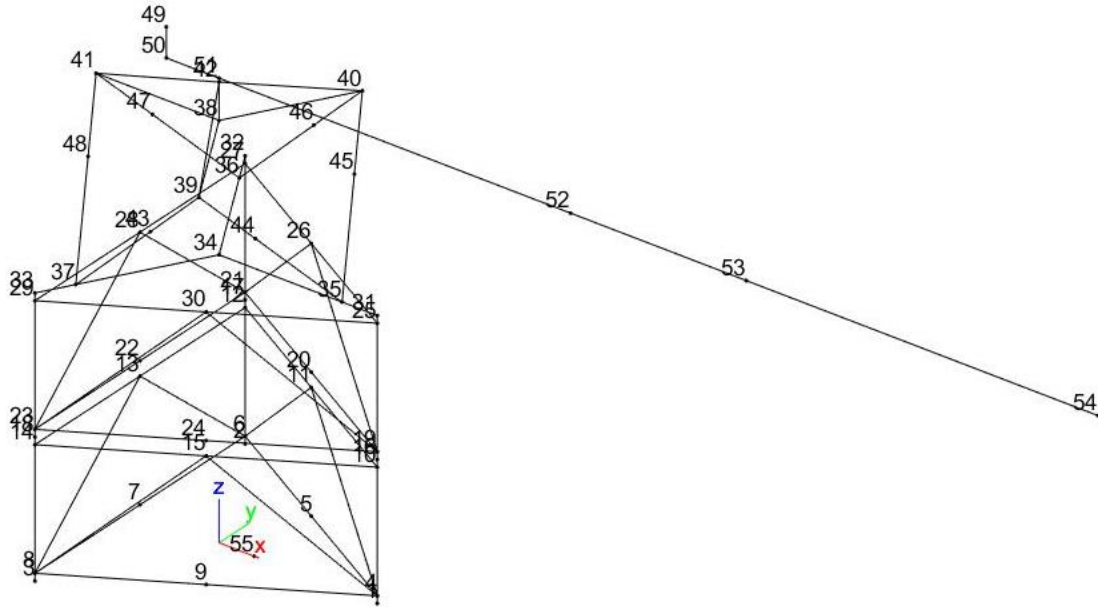


Figure 3-7: FEM model A-type system

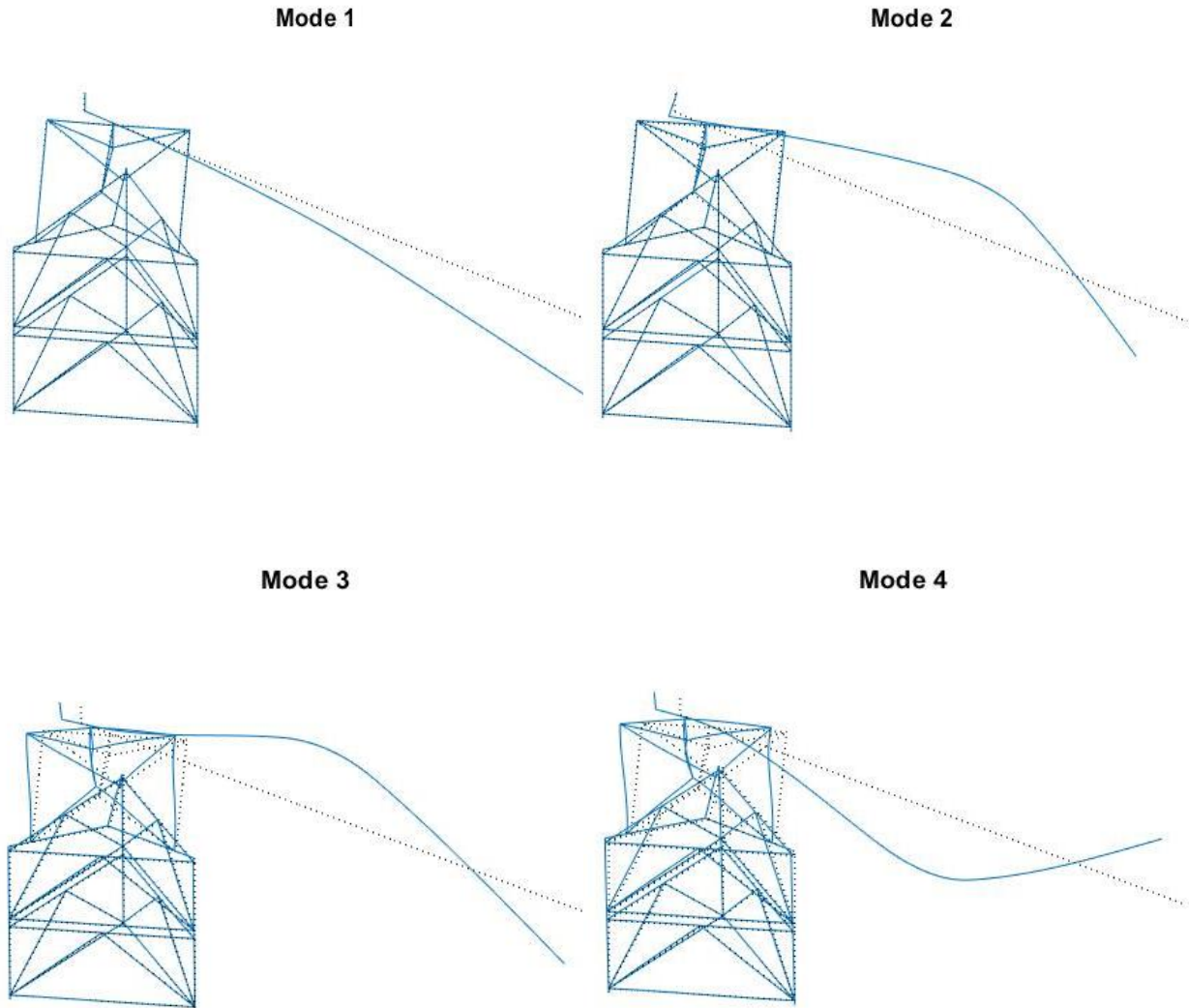


Figure 3-8: Mode shapes 1 to 4 A-type system

Table 3-1: Eigenfrequencies A-type system

Mode	Eigenfrequency A-type [Hz]
1	0.54
2	2.25
3	3.19
4	3.95

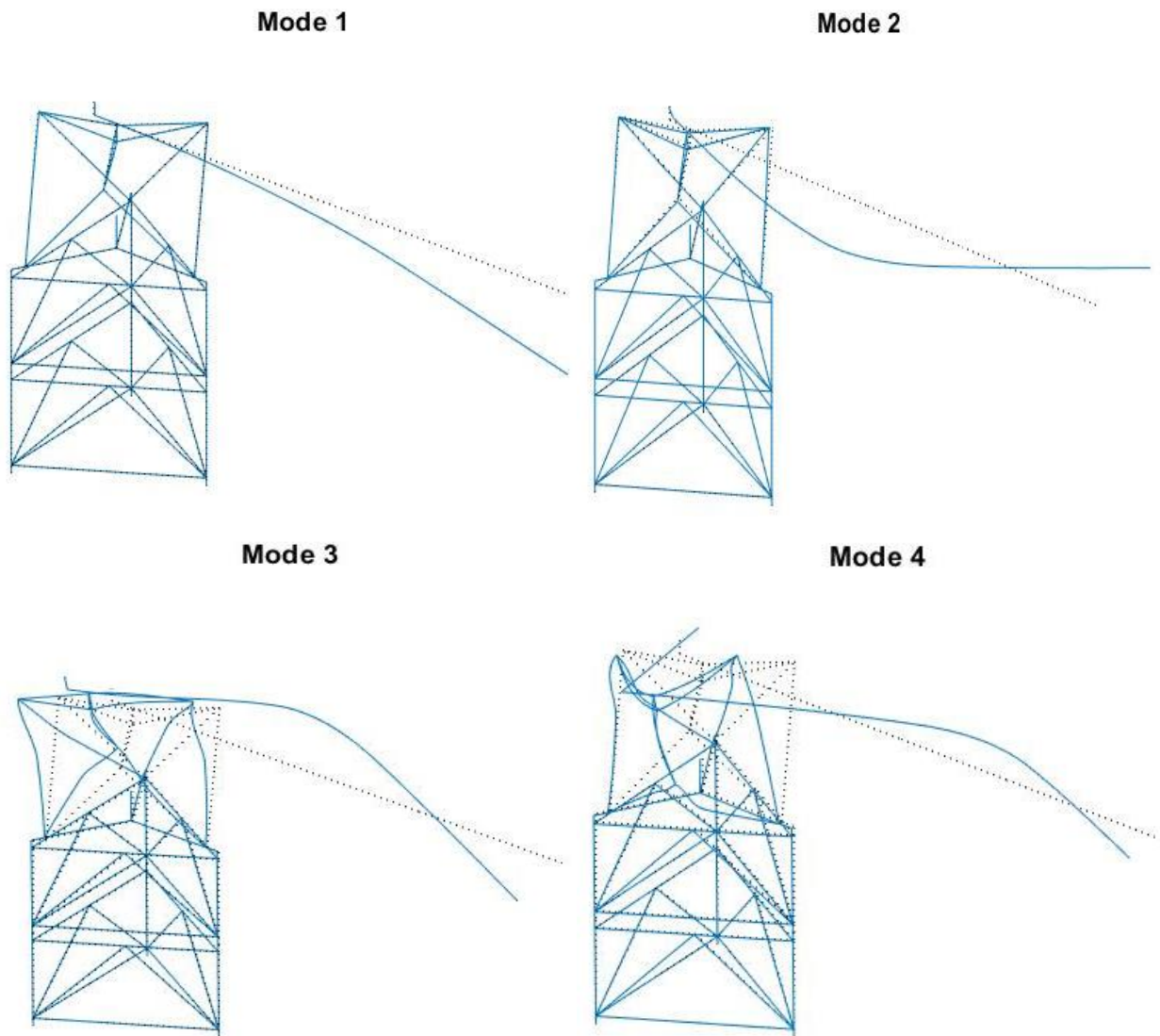


Figure 3-10: Mode shapes 1 to 4 E-type system

Table 3-2: Eigenfrequencies E-type system

Mode	Eigenfrequency E-type [Hz]
1	0.44
2	1.73
3	2.18
4	2.70

3.4 Concluding remarks

A discrete-element model of both the hexapod systems are created to determine the eigenfrequencies of the systems. The models are created using MATLAB and the toolbox StaBIL 2.0. All the elements of the system are modeled as beams except the hydraulic actuators. The properties of elements which represent the hydraulic actuators are calculated separately using a modelling study on stiffness characteristics of hydraulic cylinder under multi-factors [7]. The first four eigenfrequencies of both types of system, based on the model, are given in Table 3-3. Analyzing the eigenfrequencies and the eigenmodes of both the systems, the first two eigenfrequencies seem to be dominated by gangway vibrations. These eigenfrequencies correspond eigenfrequencies calculated in an earlier theoretical study done at Ampelmann about fatigue life of a gangway [10].

Table 3-3: Eigenfrequencies Ampelmann systems

Mode	Eigenfrequency A-type [Hz]	Eigenfrequency E-type [Hz]
1	0.54	0.44
2	2.25	1.73
3	3.19	2.18
4	3.95	2.70

4. Experimental research

To identify possible causes for the unexpected vibrations, measurements are performed on Ampelmann systems. The goal of this chapter is performing an investigation into the unexpectedly occurring vibrations. First experimental theory needed for this investigation is discussed, next data which is already available is analyzed. Based on this analysis, possible causes are determined. Next some calculations and two sets of experiments are performed investigating the possible causes.

4.1 Experimental frequency analysis

In general, frequency analysis in the field of vibration analysis is based on the discrete Fourier transform (DFT). This is a method used to transform measured samples into a frequency spectrum. The discrete Fourier transform is defined as [11]:

$$X(k) = \sum_{n=0}^{N-1} x(n) * e^{-j2\pi kn/N} \quad (4.1)$$

The inverse discrete Fourier transform (IDFT) is defined as:

$$x(n) = \frac{1}{N} \sum_{k=0}^{N-1} X(k) * e^{j2\pi kn/N} \quad (4.2)$$

When the following sampled signal is assumed: $x(n) = x(n\Delta t)$ and N samples, which is called the blocksize, have been collected. N is usually taken to be an integer power of two (2^p) to use and optimize the fast Fourier transform algorithm (FFT). This is an algorithm which computes the DFT in a faster way then using equations 4.1 directly.

4.1.1 Discrete Fourier transform

In Figure 4-1 a summary of the DFT is given. This summary is based on [11]. First a continuous signal (A.1) is transferred to the frequency domain (B.1) using the regular Fourier transform. The next step is to sample the time signal (A.2 and A.3). This is equivalent to multiplying the continuous signal by an ideal train of pulses with an unit value at each sampling instant and otherwise zero. In the frequency domain this operation corresponds to the convolution with the Fourier transform, which in this case is a train of pulses at multiples of the sampling frequency (B.2 and B.3). Measurements are only performed during a finite period in time, which is a multiplication of the continuous signal with a rectangular window (A.4 and A.5). In the frequency domain this is equivalent to the convolution with a sinc function: $sinc(x) = sin(x)/x$ (B.4 and B.5). The result of this truncation is uncertainty in the frequency domain, which can be seen by the ripple of the spectrum in (B.5). The final step is carried out in the frequency domain (B.6 and B.7). The DFT only calculates the spectrum at discrete frequencies, i.e. it is a multiplication of the spectrum with a train of pulses with a frequency increment of $\Delta f = 1/T$. In the time domain (A.6 and A.7) this step is equivalent to the convolution of a train of pulses with a separation of T.

4.1.2 Spectrum averaging

Many measurement signals contain random noise, either because the signal is random, or because it is periodic or transient but contains contaminating noise. When this is the case, spectra are often averaged frequency by frequency to reduce the random error of the spectrum estimate. The entire time signal is divided into M segments (Figure 4-2). Of each segment the DFT is calculated. The squared magnitude value for each frequency is averaged. In case of periodic or transient signals typically 3 – 10 segments are necessary. Overlapping processing means using the same time sample more than once, so the final value will contain more DFT results from the same data. This process gives a better result because the time window used before the DFT calculation removes some information at the ends, where the window approaches zero. The amount of overlap that should be used depends on the time window. With the Hanning window, which is used, an overlap of 50% is usually seen as optimal [12].

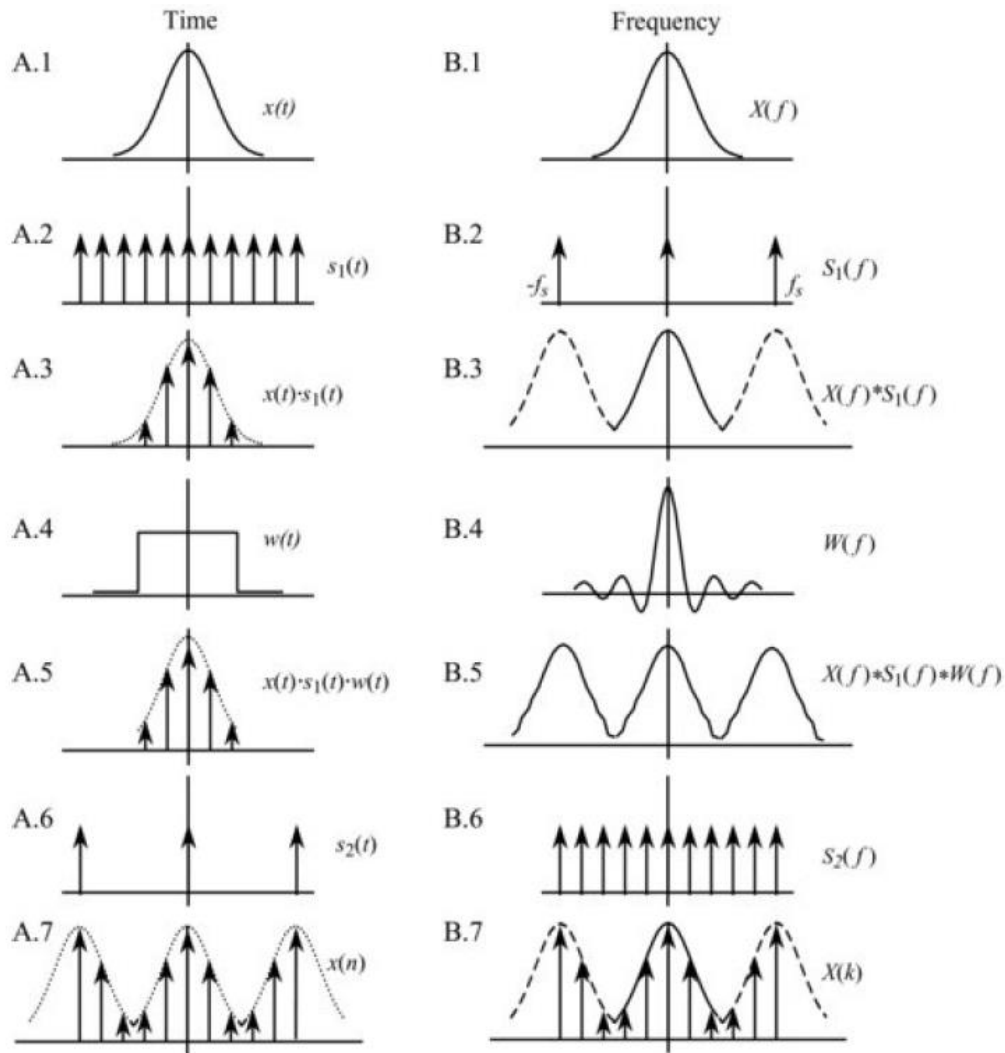


Figure 4-1: Summary of discrete Fourier transform [11]

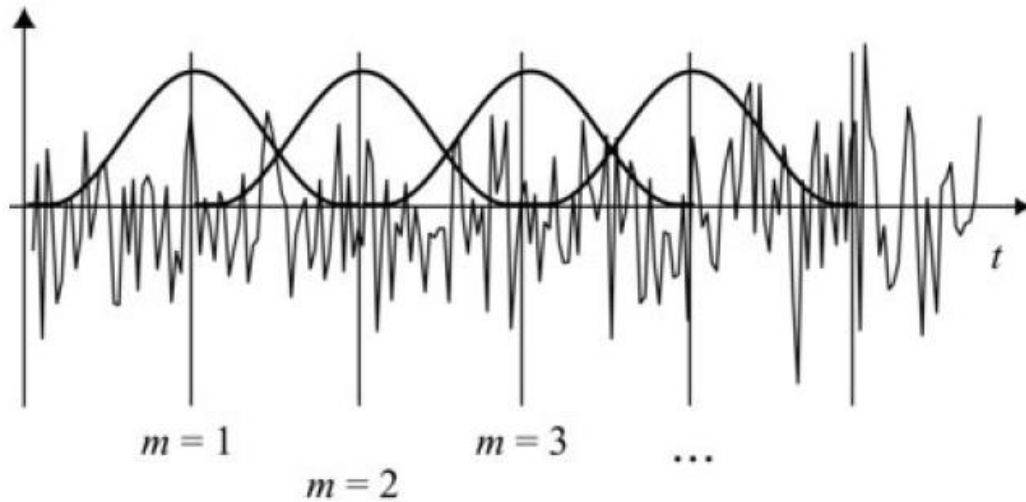


Figure 4-2: Segment-based frequency domain averaging [12]

4.1.3 Forward kinematics of a Stewart platform

The Stewart platform mechanism is a parallel kinematic system that can be used as the basis for controlled motion in six degrees of freedom. The mechanism consists out of a stationary platform and a mobile platform connected via, in the case of Ampelmann, six hydraulic actuators. The desired position and orientation of the mobile platform is achieved by combining the lengths of the six struts, transforming the six transitional degrees of freedom into three positional and three orientational ones. The lengths of the actuators cannot be changed independently, but only in a way that the hexapod construction allows [1]. The main difficulty with parallel manipulators is the complexity of controlling their movement. The inverse kinematics (see paragraph 2.2.2) can be defined as finding the actuator lengths needed to position the mobile platform in a desired position. The solution to this problem is not complex and can be computed in a short time. The forward kinematics of a parallel manipulator is finding the position and orientation of the mobile platform when the actuator lengths are known. This problem has no known closed form solution [13].

The forward kinematics of a hexapod system can be formulated mathematically in several ways. Every representation of the problem has its advantages and disadvantages which become clear when a different optimization algorithm is applied. The forward kinematics given below are based on [13]. The most common approach, which is also the one used by Ampelmann, uses three positional coordinates of the center of the mobile platform (t) and three angles to define its orientation. The hexapod geometry is defined with six vectors for the base platform (b_i) and six vectors for mobile platform (p_i), which define the six joint coordinates on each platform. The actuator vector (l_i) is expressed in equation 4.3, where R is a rotation matrix calculated from the rotation angles.

$$l_i = -b_i + t + R * p_i \quad (4.3)$$

For an arbitrary solution to the forward kinematics problem the error can be expressed as the sum of the squares of the difference between the calculated lengths and the actual values (see equation 4.4), D is the distance between each vector pair. This results in an optimization function which relates all the unknowns. This function is non-linear due to the trigonometric function in the rotation matrix. However, the function is derivable and is the most common representation of the forward kinematics problem.

$$f = \sum_{i=1}^6 (D(b_i, t + R * p_i)^2 - l_i^2)^2 \quad (4.4)$$

4.2 Pre-processing

The Ampelmann system contains a lot of sensors. The data they provide is continuously stored, for a period of two weeks, and available through the Ampelmann system data network (ASDN). The Ampelmann system uses two motion reference units (MRUs), where one functions as a redundancy for the other. The two sensors are located on the bottom frame (Figure 4-3). Also, the length of the cylinders is measured over time. The Ampelmann system is not able to compensate for all the motions resulting in some residual motions. In the figures discussed in this paragraph for clarity only part of the measured signal, namely one window as explained in paragraph 4.1, is shown in the time series.

4.2.1 A-type and E-type

In Figure 4-4 and Figure 4-5 the normalized translations and rotations for two A-type Ampelmann systems are plotted in the frequency domain. Both systems are installed on identical vessels. However, the A-28 is installed on the ship deck of the Esvagt Froude, while the A-29 is placed on a pedestal on the Esvagt Faraday (see appendix D). In Figure 4-7 and Figure 4-8 the normalized translations and rotations for two E-type Ampelmann systems are plotted in the frequency domain. One of the systems is placed on a pedestal (E-04) on the Siem Barracuda while the other is attached to the ship deck (E-14) on the Olympic Orion (see appendix D). The vessel on which the systems are located differ from each other, so the comparison is not as good as for the A-type system. For both of the systems the motions in the time domain are plotted in appendix C.

For all the systems, in the frequency domain a JONSWAP spectrum can be distinguished between roughly 0 Hz and 0.75 Hz as a result of the vessel motions. The energy in the frequency range between 0.75 Hz and 6 Hz for the systems placed on a pedestal (A-29 and E-04) is higher and more distributed than for the system placed on the deck (A-28 and E-14). Indicating motion not directly related to vessel motions. For the system located on the deck four clear peaks are visible at 2.3 Hz, 2.6 Hz, 4.8 Hz and 5.1 Hz.

In Figure 4-6 and in Figure 4-9 the difference between the two MRUs for the two A-type systems and E-type system in heave are plotted in the time and frequency domain. Most of this difference is located in the lowest part of the spectrum (0 Hz – 0.03 Hz). Some clear peaks for the system attached to the ship deck again are visible in the relative higher frequency range (1 Hz – 6 Hz) at the same frequencies as in the heave direction.

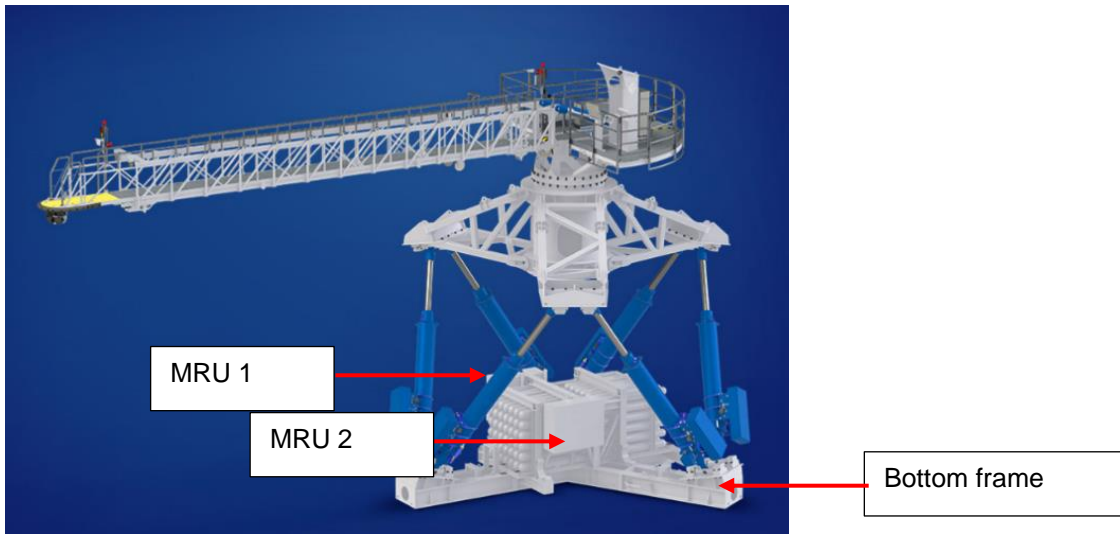


Figure 4-3: Location of the motion sensors

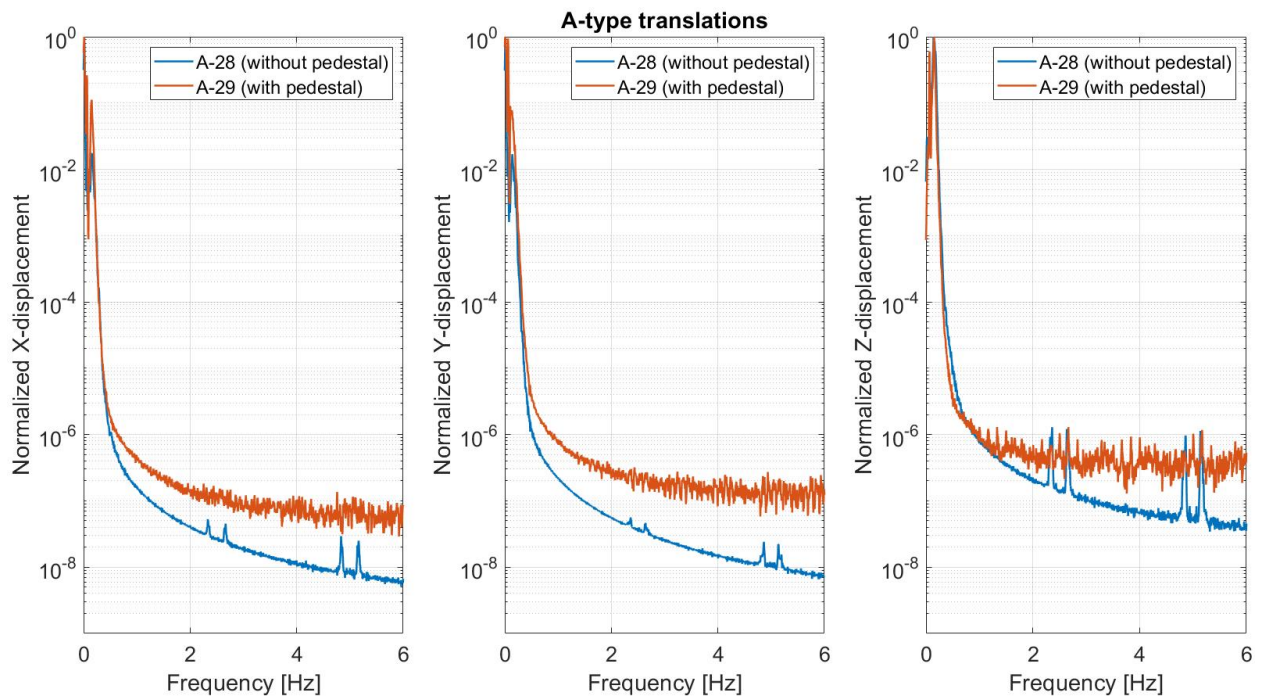


Figure 4-4: Translations A-type systems

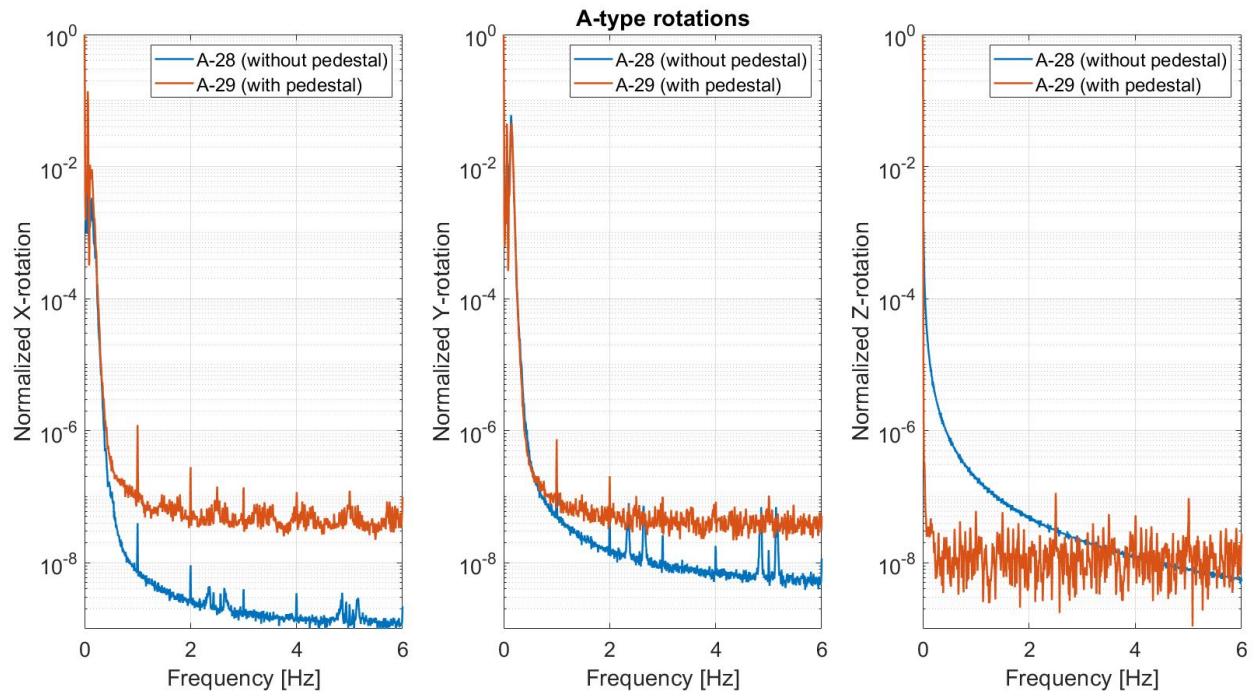


Figure 4-5: Rotations A-type systems

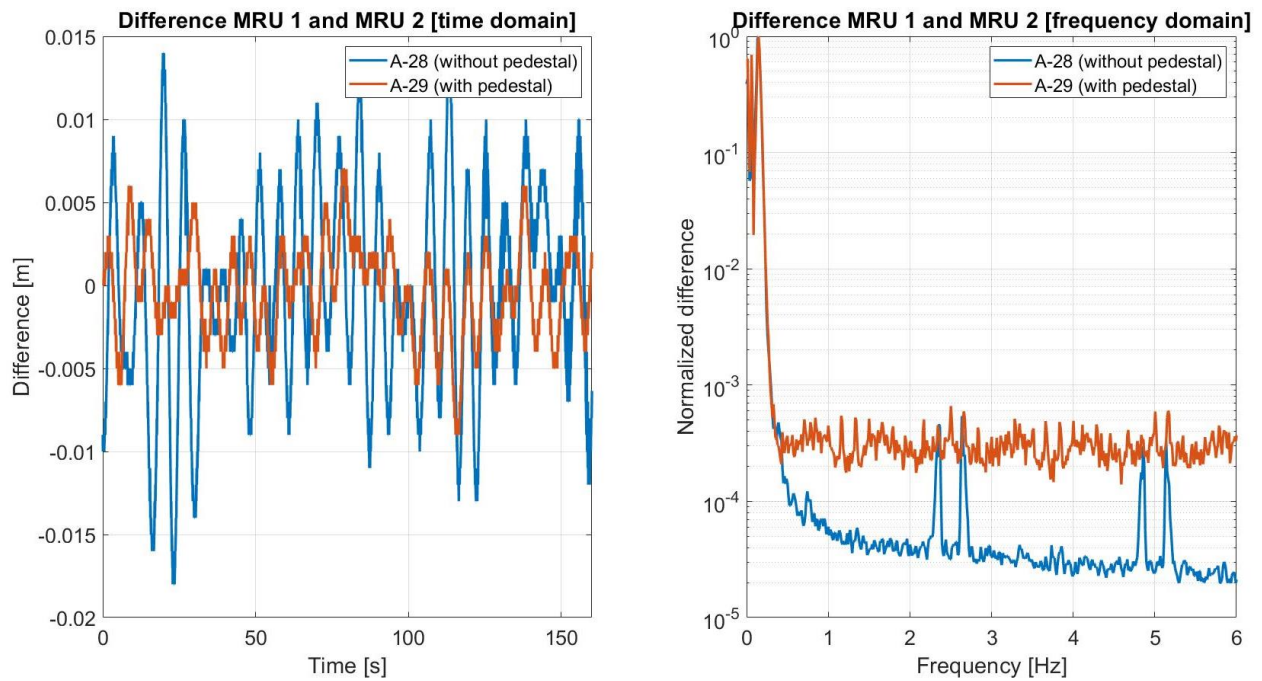


Figure 4-6: Difference between MRU 1 and MRU 2 in heave direction for A-type systems

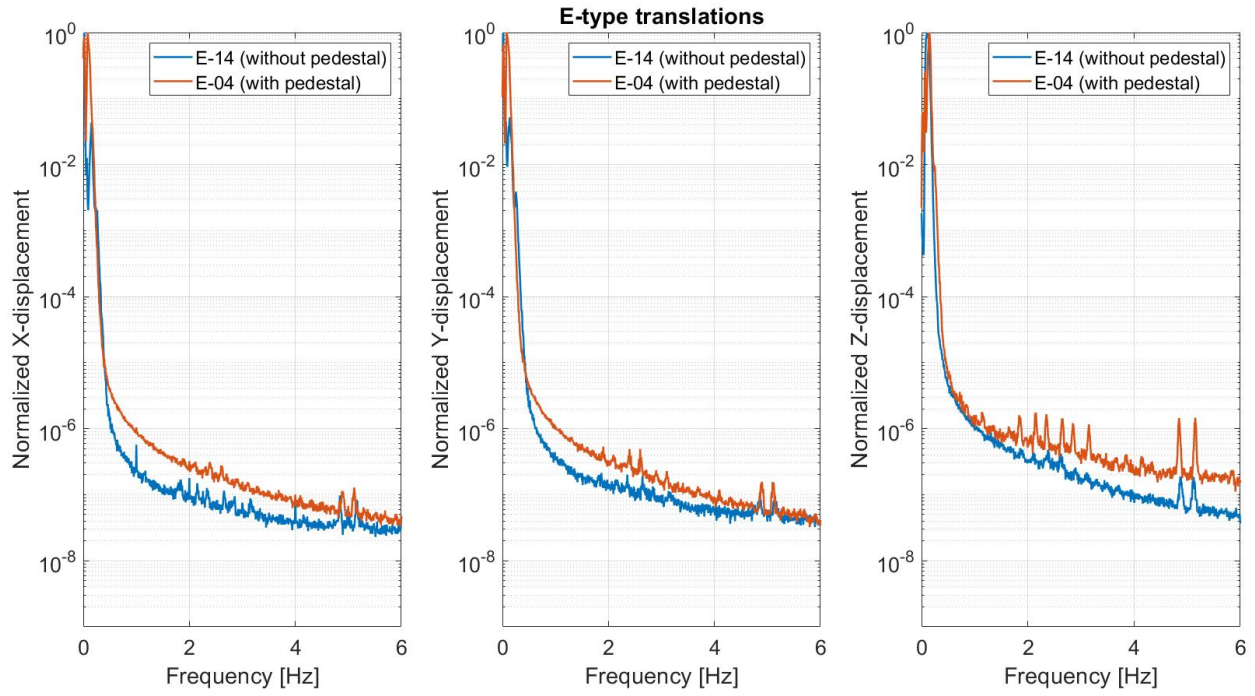


Figure 4-7: Translations E-type systems

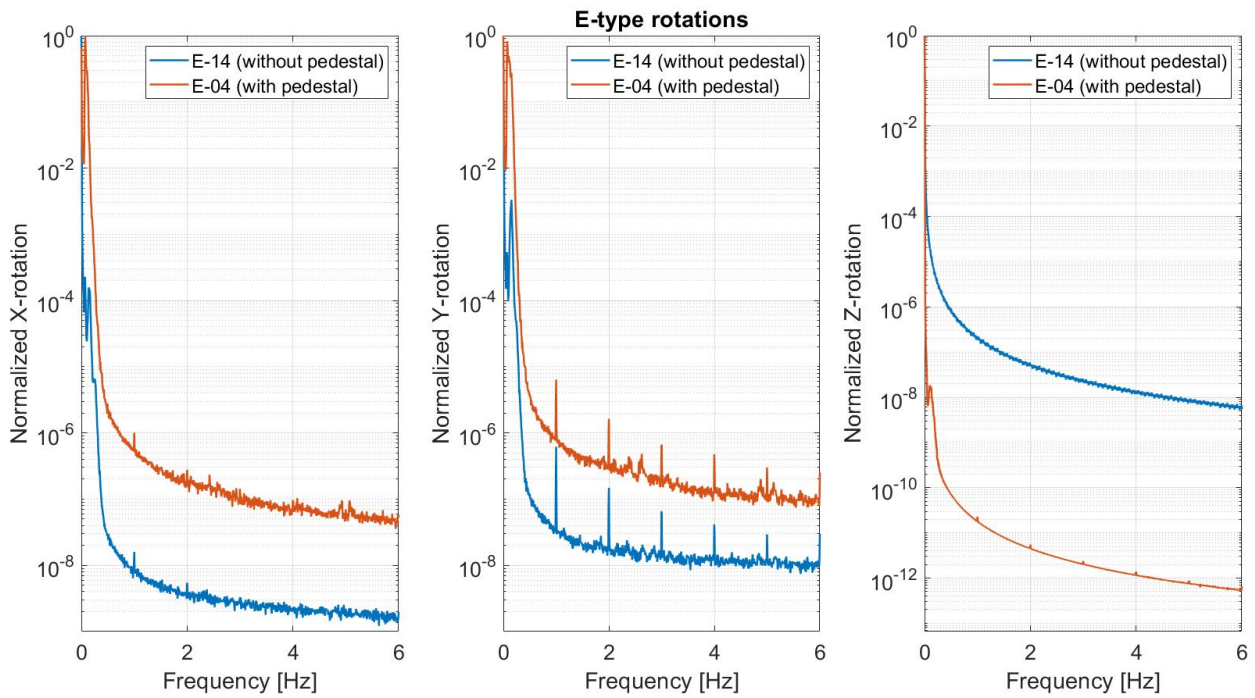


Figure 4-8: Rotations E-type systems

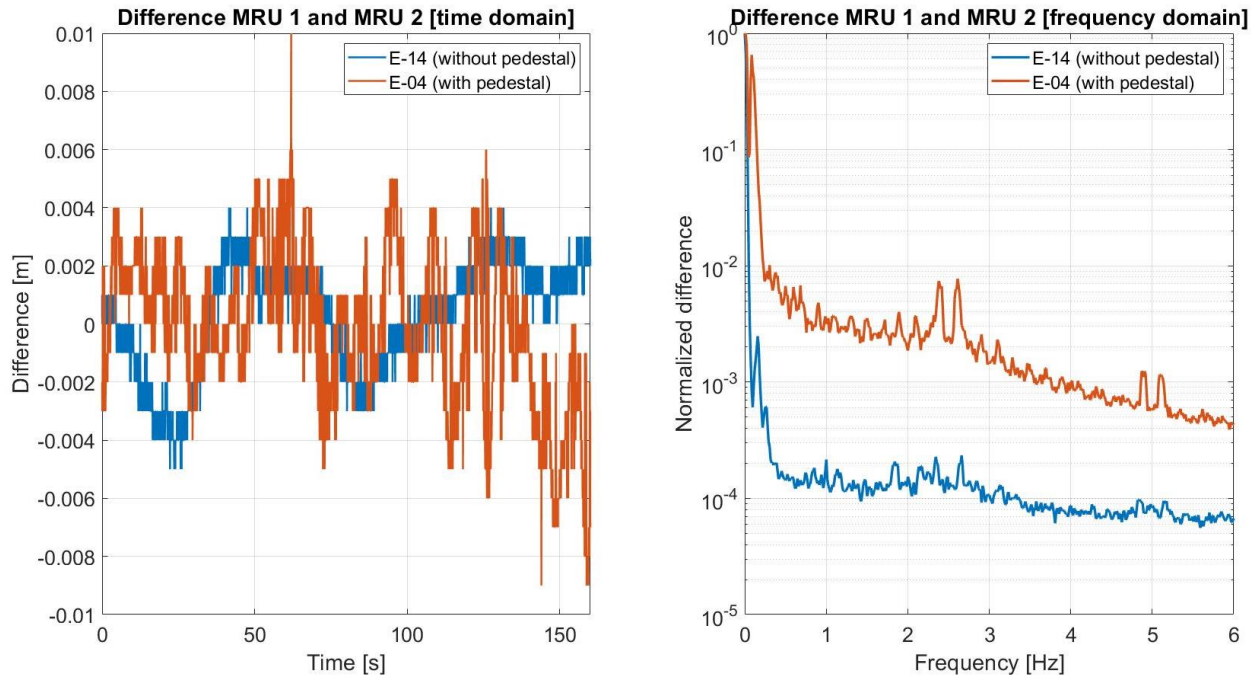


Figure 4-9: Difference between MRU 1 and MRU 2 in heave direction for E-type systems

4.3 Possible causes of unexpectedly occurring vibrations

In Figure 4-10 a schematic overview of an Ampelmann system is given. Based on paragraph 4.2 three possible causes are determined. These possible causes come down to investigating the influence of the parts above (gangway) the hexapod, the influence of parts of the system below (pedestal) the hexapod and the working limits of the Ampelmann system resulting in residual motions.

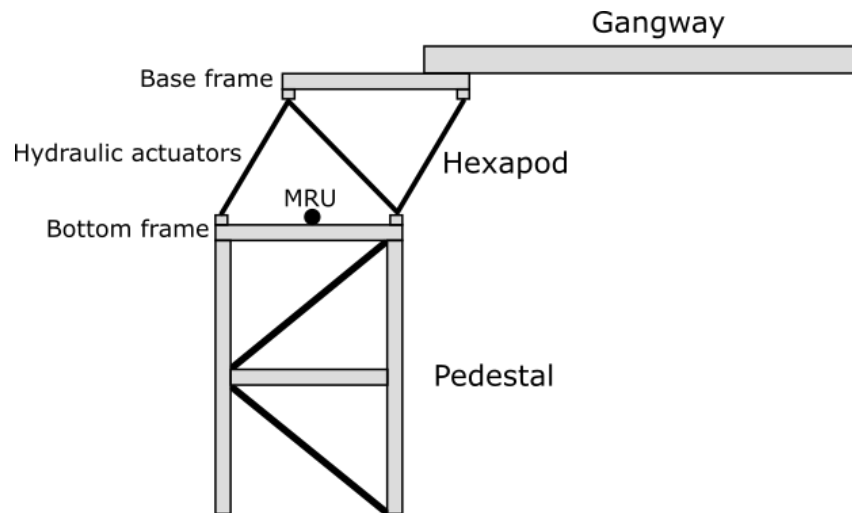


Figure 4-10: Overview Ampelmann system

4.3.1 Influence of the pedestal

In Figure 4-11 a schematic cross section of an Ampelmann system on a pedestal is given. When the pedestal is excited and starts vibrating the system will try to compensate for these. However, these extra motions are not directly related to vessel motions. In Figure 4-4, Figure 4-5, Figure 4-7 and Figure 4-8 the six degrees of freedom of an A-type and E-type Ampelmann system, placed on a pedestal and attached to the ship deck, are plotted in the frequency domain. In all the degrees of freedom the influence of the pedestal is clearly visible. More energy is contained in the relative higher frequencies (0.75 Hz – 6 Hz). These motions are measured by the MRUs which results in the system trying to compensate for these motions. This might result in a vicious circle resulting in unintended vibrations in the systems. The following will be investigated:

Compensating for motions caused by vibrations in the pedestal can cause the unexpected vibrations in an Ampelmann system.

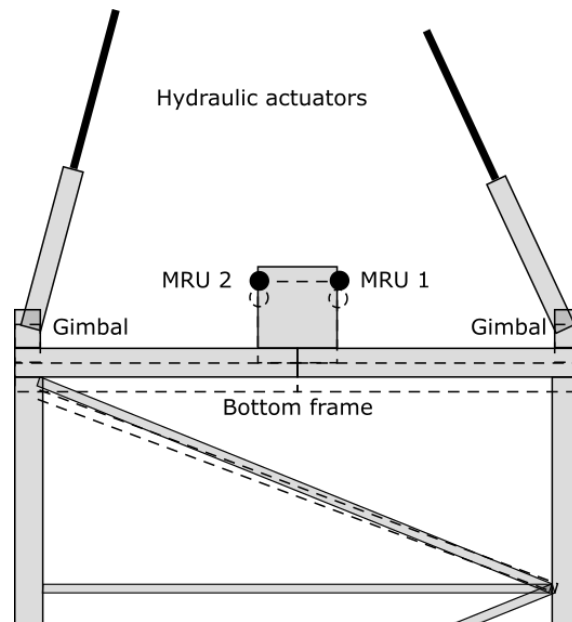


Figure 4-11: Cross section of Ampelmann system; vibrations caused by a pedestal

4.3.2 Residual motions

Due to the limitations of the Ampelmann system some residual motions exist (Figure 4-12), which means the transfer deck and gangway are not fully compensated. For example: the cylinders of the Ampelmann systems have a limited range. The cylinders must be prevented from running in to their buffers. Because of this the cylinders are never controlled to more than 80 % of the maximum rake. Secondly when the cylinders are over 50 % of their rake, the system starts to partially compensate for the measured motions. Also, the frequency filter in the motion control algorithm (Figure 2-3) can cause lag. These cause residual motions. When peaks in the frequency domain of these motions correlate to the eigenfrequencies of the transfer deck and gangway, vibrations can occur. The following will be investigated:

The frequency content of the residual motions corresponds to the eigenfrequencies of the gangway which can cause the unexpected vibrations in an Ampelmann system.

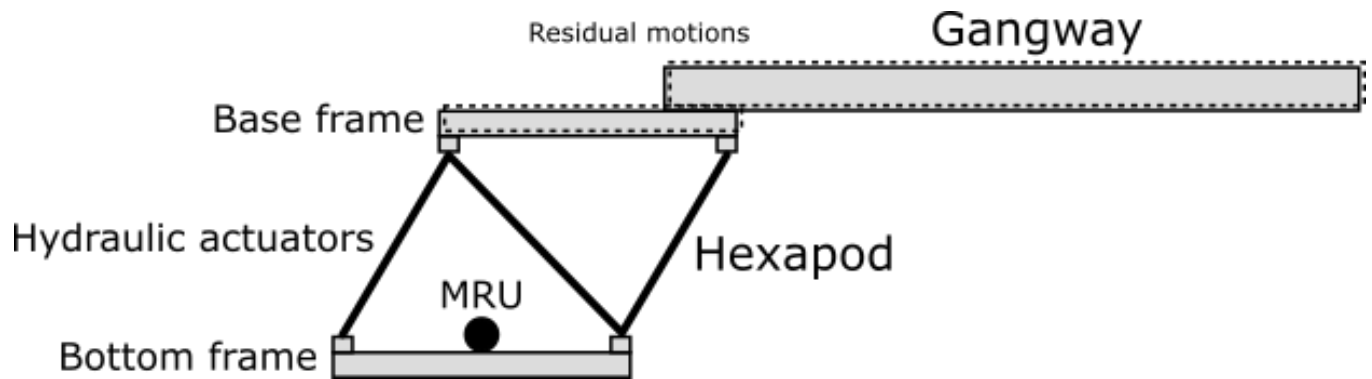


Figure 4-12: Cross section of Ampelmann system; residual motions

4.3.3 Vibrations in the bottom frame due to compensating for gangway motions

In Figure 4-13 a schematic cross section of an Ampelmann system is given. The pushing and pulling of the hydraulic cylinders against their gimbals results in a response in the bottom frame. As a result, the bottom frame will deform resulting in motions in the MRUs. In Figure 4-6 and Figure 4-9 the difference between the two MRUs in heave direction is plotted. In these figures the fluctuations in the time domain might indicate vibrations in the bottom frame. When the Ampelmann system starts compensating for motions with the same frequency as the eigenfrequency of the bottom frame, large motions might arise. These motions are measured by the MRUs which leads to the system trying to compensate for these motions. This might result in a vicious circle introducing unintended vibrations in the systems. The following will be investigated:

Vibrations in the bottom frame due to compensating for gangway motions can cause the unexpected vibrations in an Ampelmann system.

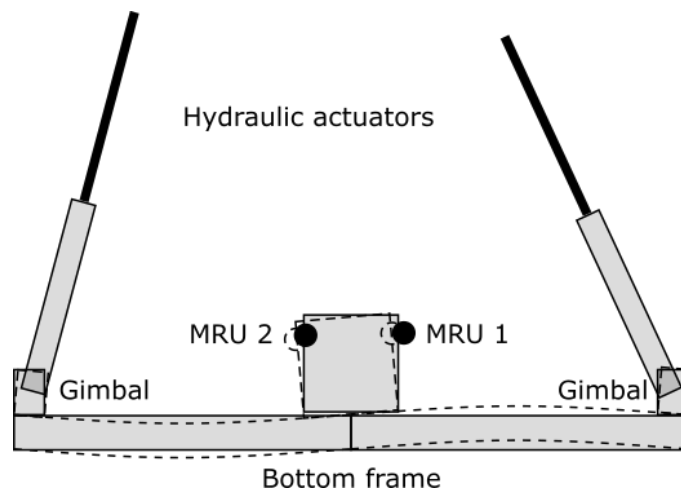


Figure 4-13: Cross section of Ampelmann system; vibrations in the bottom frame

4.4 Measurements on the Ampelmann system

An experiment can be classified based on the input or loading using the following: Is the input dynamic or static? Is the input controllable and whether the inputs are measurable. An experimental procedure can be roughly divided into a number of steps [14]. These steps are:

1. Selection of inputs, their locations and their means of measurement.
2. Selection of outputs, their locations and their means of measurement.
3. Gathering and transmission of signals to a recorder/logger.
4. Conversion of the signal to a storable form.
5. Data storage

The sensors which will be used for measuring during the different tests are all iXblue Octans (look for technical specifications in appendix E). This is the same MRU which is used on the Ampelmann systems. The Octans is a gyrocompass and motion sensor measuring displacements and accelerations in six degrees of freedom. The Octans is a fiber optic gyroscope. In these types of gyroscope, pulses of light are sent through windings of fiberglass, both clockwise and counterclockwise. When the sensor rotates, a tiny difference can be measured in the arrival time of the light pulses, when comparing the clockwise pulses with the counterclockwise pulses.

All signals measured on mechanical systems are defined continuous in time. When they are recorded, they are measured in time discrete signals with a sampling frequency. The sampling frequency of the sensor is set at 50 Hz. According to the Nyquist frequency, the sampled signal, which is continue, can only be uniquely represented by discrete samples if it is sampled using a frequency larger than twice the highest frequency in the analogue signal. This means that the lowest frequency to be investigated is 25 Hz. This is well above the frequencies of the vibrations which are the subject of investigation.

4.4.1 Influence of the pedestal

To investigate the possible influence of the pedestal on the bottom frame the following test is performed: A ship to ship MRU (Figure 4-15) are placed on the ship deck. The data from the ship to ship MRU and the MRUs which are already on the system are compared. From this data the influence of the pedestal can be determined. The measurements are taken from an E-type (E-04) system. This system is placed on the Siem Baracuda (appendix D). The measurements are performed during regular operations of the system.

During this experiment the input will be the vessel motions at the base of the Ampelmann system or the pedestal. These motions are uncontrollable but measurable. The output will be the system responses. The measurements are done using the MRUs of the Ampelmann system and a ship to ship MRU. The gathering of the data is done using CPU of the Ampelmann system. This makes sure all the signals are synchronized time wise and will automatically convert the data to usable format and is stored.

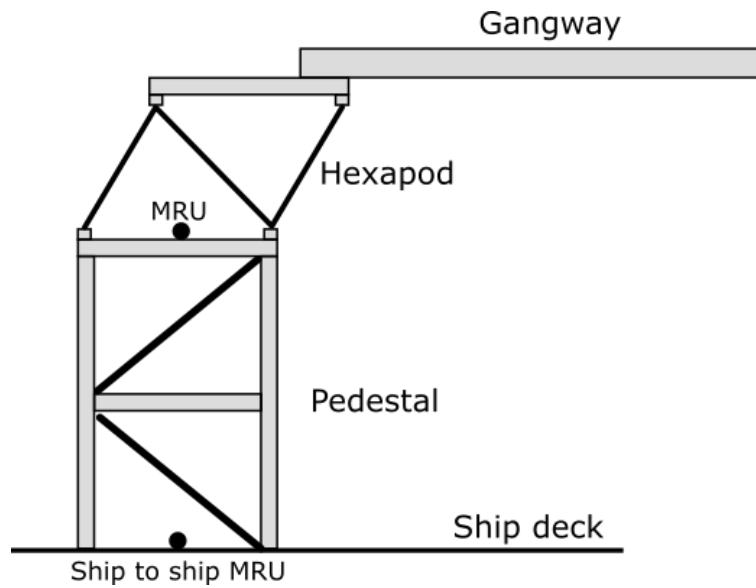


Figure 4-14: MRU locations

Dimensions: 60 x 60 x 22 cm (HxWxD)
 Power requirements: 230V 50Hz (max 3A)
 Radio signal: 2,4GHz (range 50-250m)



Outside of S2S-box (front)



Inside of S2S-box

Figure 4-15: Ship to ship MRU

Results

In Figure 4-17 the translations and in Figure 4-18 the rotations in the time domain of the two MRUs are plotted. The rotations for both the MRUs are roughly the same (for the difference see appendix F). The trend and the amplitude are reasonably the same. However, this is not the case for the translations. This is because the motions measured by the MRUs are translated to the center of gravity of the Ampelmann system. This is done using lever arm as indicated in Figure 4-16 by dX and dZ . The lever arm of the MRU, which is fitted on the system, is precisely known. Determining the exact lever arm for the ship to ship Octans proved to be difficult. Because the lever arm for the ship to ship MRU are large, the translations for the most part are determined by the rotations of the MRU. When the lever arm are not precisely correct, the translations will contain an error.

In Figure 4-19 translations and in Figure 4-20 the rotations in the frequency domain are plotted. The energy of the motions measured by the regular MRU, which includes the pedestal, contains more energy in the relative higher frequencies when compared to the ship to ship MRU. This is the same as in paragraph 4.2. The peaks in the frequency graphs are roughly located at: 2,8 Hz, 5,4 Hz and 8,1 Hz for all the degrees of freedom. This is because the data measured by both the MRUs is measured with respect to a fixed coordinate system. As a consequence, the motions of the pedestal have an influence in multiple directions in the MRU's local coordinate system. Another consequence of this dependency is that Figure 4-19 and Figure 4-20 are similar.

Four peaks can be identified in both the signals. The first is directly caused by vessel motions so a JONSWAP spectrum. The other three have a cause which is not directly related to vessel motions. The second and third peak have roughly the same amplitude for both the data sets. However, the fourth peak of the system MRU Octans 1 has a much larger amplitude compared to the amplitude of the ship to ship Octans. Around the frequency of this peak, 8,1 Hz, more energy is present at the top of the pedestal than at the bottom. For this frequency the pedestal seems to amplify the energy present at the ship deck.

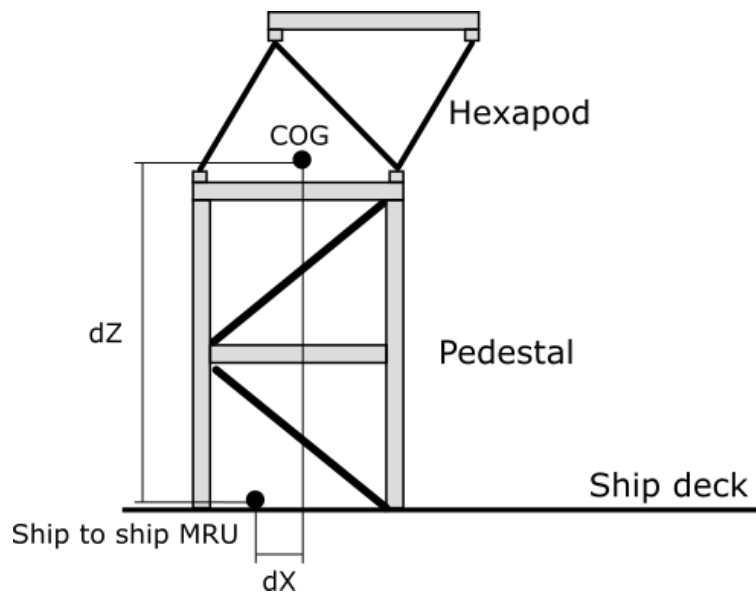


Figure 4-16: Lever arms (dX & dZ)

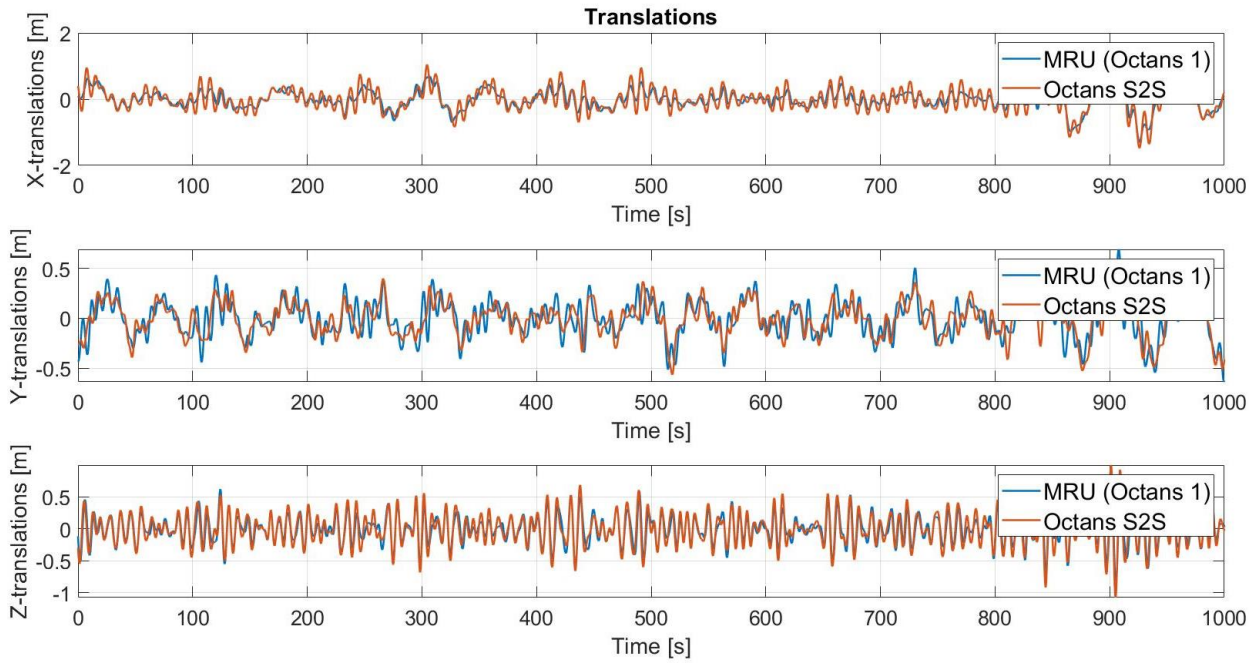


Figure 4-17: E-04 Translations (time domain)

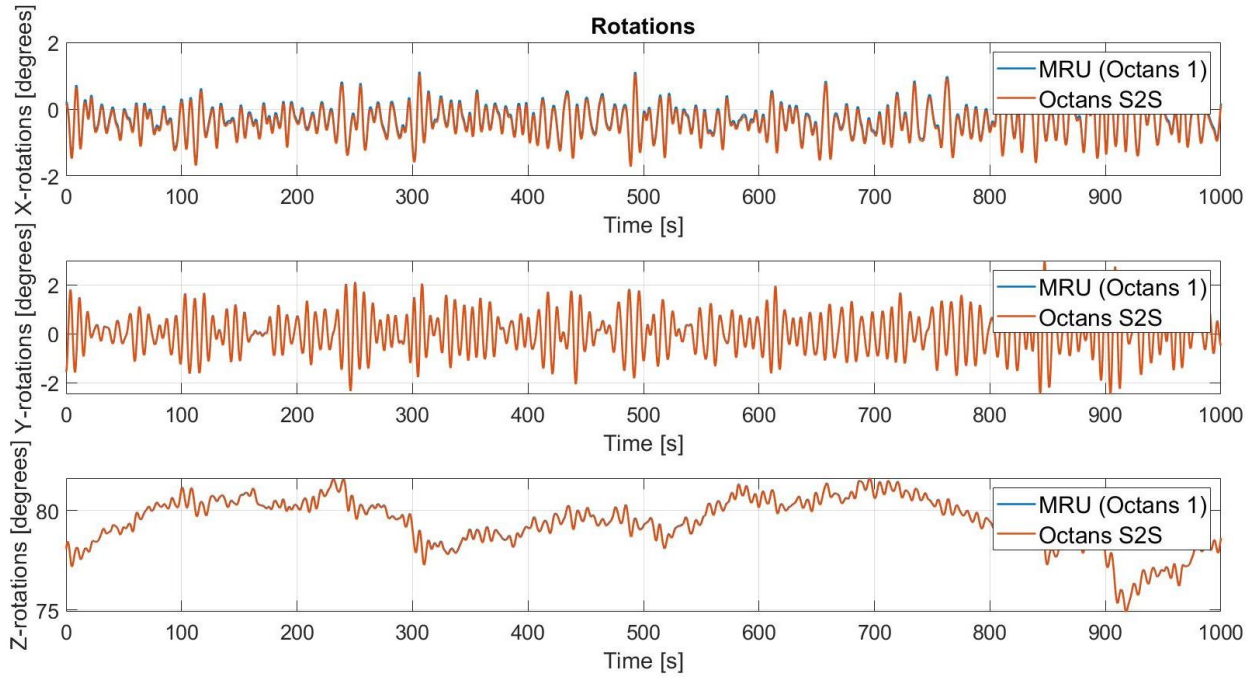


Figure 4-18: E-04 Rotations (time domain)

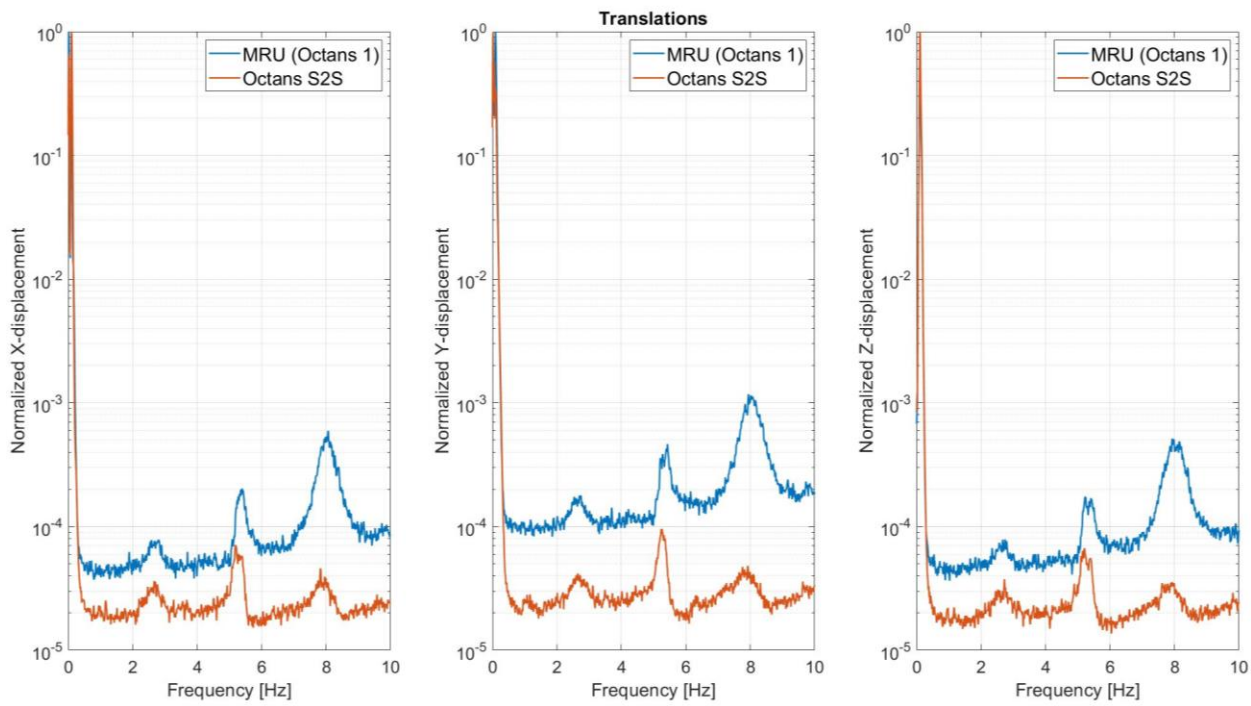


Figure 4-19: E-04 translations (frequency domain)

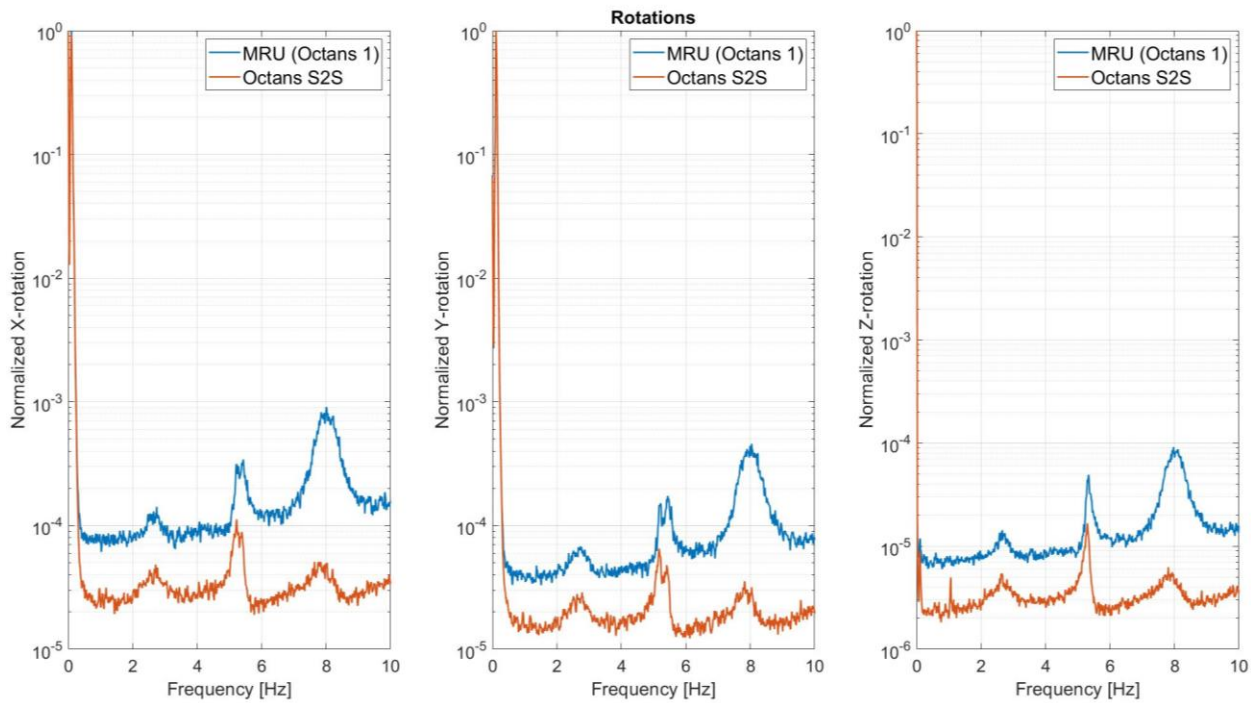


Figure 4-20: E-04 Rotations (frequency domain)

Possible cause

As in the previous paragraph is stated, the pedestal seems to amplify energy present at the ship deck. A possible explanation for this phenomenon could be found in the eigenfrequencies and corresponding eigenmodes of the ship deck. In Figure 4-21 a schematic drawing showing this characteristic is given. The ship deck bends according to a certain mode shape. The pedestal functions as an arm increasing the amplitude of the motion of the Ampelmann system on top. The system will try to compensate for these motions. The compensation for this motion will occur with the same frequency as the eigenfrequency of the ship deck adding more energy at this frequency to the system. This might result in a vicious circle resulting in unintended vibrations in the systems.

The different stiffeners in a ship deck of a crane vessel close to a heavy-duty crane are in general much heavier than the stiffeners below the main deck to cope with the forces introduced by the crane. In general, the Ampelmann system is placed on the main deck of a vessel not specifically engineered to cope with the system. An Ampelmann system introduced roughly the same dynamic forces as a crane. This supports the idea that vibrations in the ship deck might cause the unexpected vibrations.

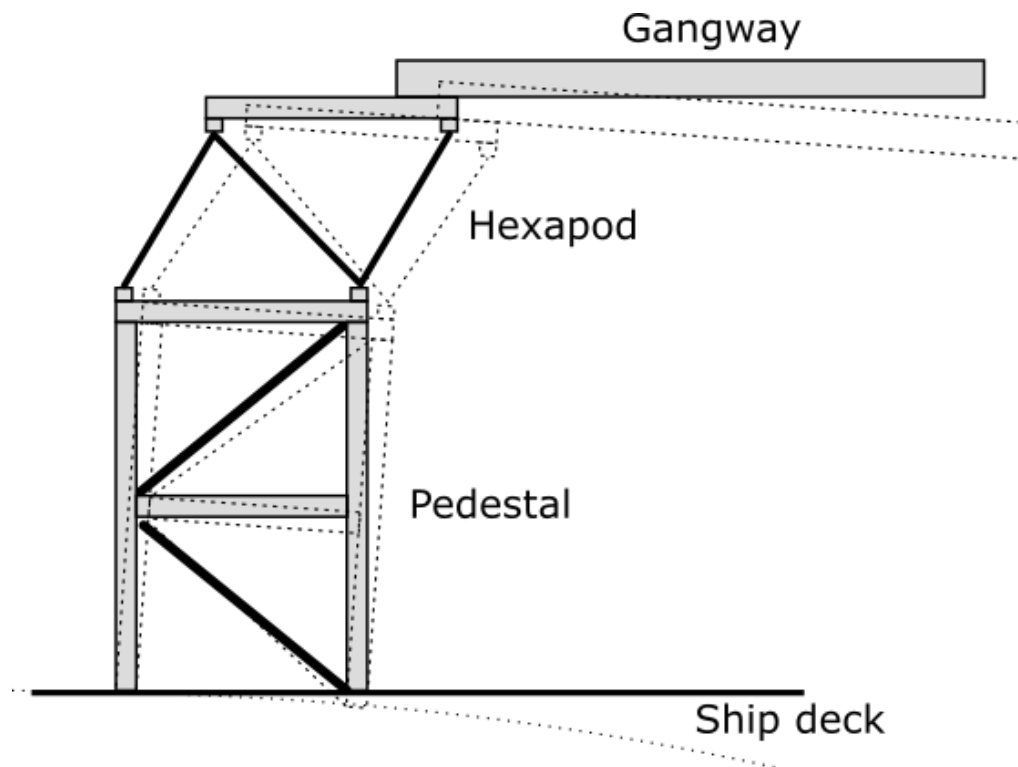


Figure 4-21: Schematic overview ship deck vibrations

4.4.2 Residual motions

To investigate the possible influence of the residual motions and if they can cause the vibrations, these residual motions are calculated. For these calculations the forward kinematics as explained in paragraph 4.1.3 are used. The forward kinematics require as input the motions at the base of the hexapod, which is the Octans data, and the corresponding cylinder lengths (Figure 4-22). For this data again the Ampelmann system data network (ASDN) is used. To make sure sufficient residual motions are present during the sampled time, data is used while the vessel containing the Ampelmann system was in the most severe sea state available.

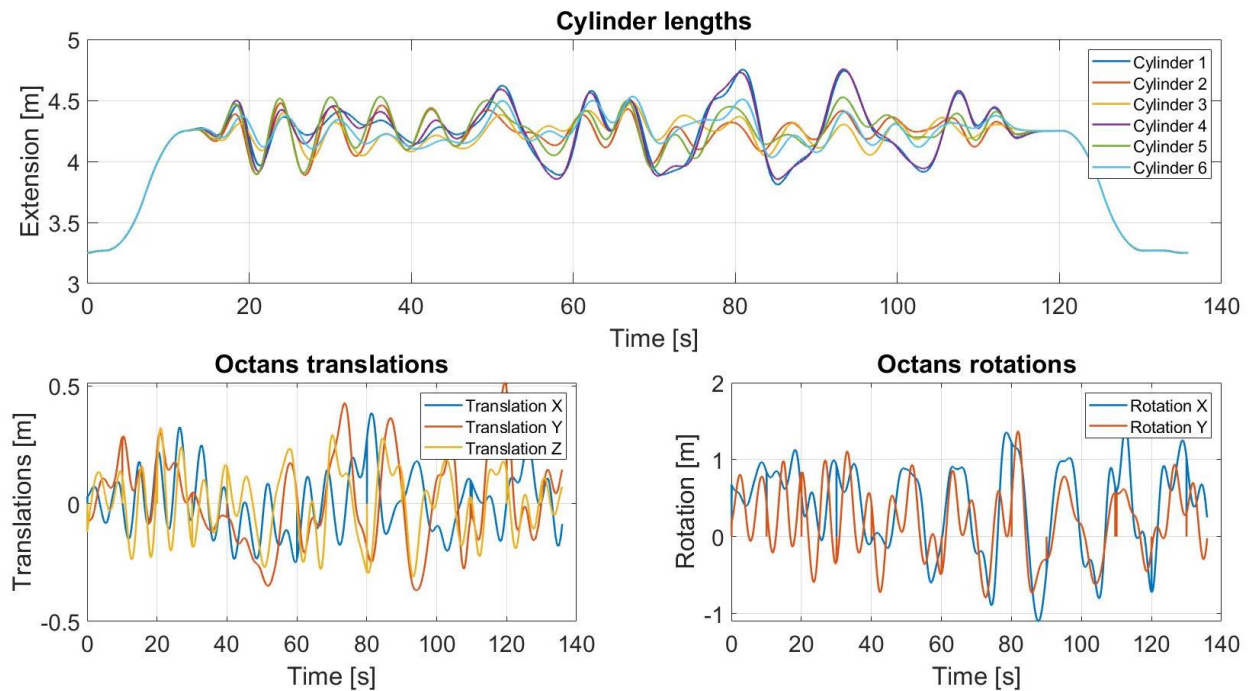


Figure 4-22: Cylinder lengths and reference motions

Results

In Figure 4-23 the residual motions in the time and frequency domain are given. In Table 4-1 the first five theoretical eigenfrequencies of a typical Ampelmann gangway are given based on a fatigue analysis done at Ampelmann [10]. The frequencies given in Table 4-1 coincide with the inverted peaks in the frequency graph. Meaning the motion control algorithm and Ampelmann system is good at compensating for vibrations with the eigenfrequency of the gangway. In the graph no amplification of energy can be distinguished. Because of this it can be concluded that the residual motions do not cause the unexpected vibrations.

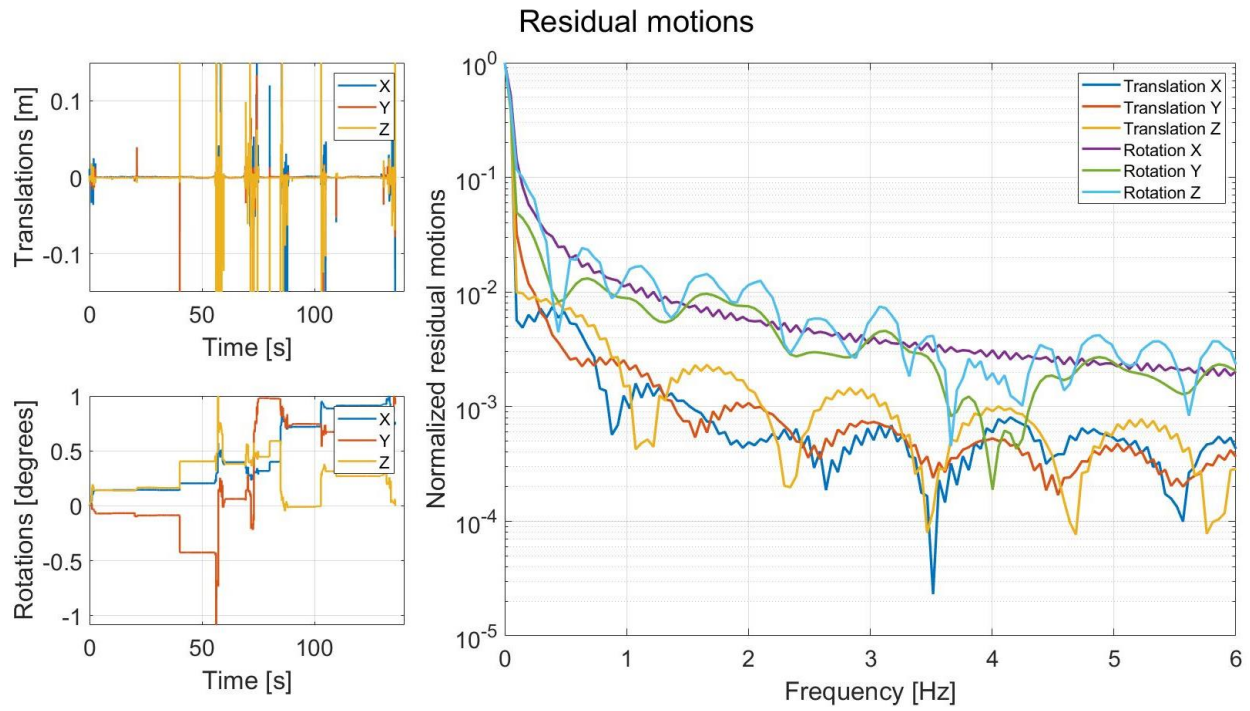


Figure 4-23: Residual motions (time and frequency domain)

Table 4-1: Theoretical eigenfrequencies gangway [10]

MODE NUMBER	EIGENFREQUENCY
1 st	0,45
2 nd	1,28
3 rd	1,64
4 th	2,19
5 th	3,02

4.4.3 Vibrations in the bottom frame

To investigate the possible influence of the gangway on the bottom frame/MRUs the following test is performed. The gangway on an A-type Ampelmann system is given an excitation using the hydraulic cylinders normally used for luffing. This resembles the effect of hitting a beam with a hammer. The gangway will start vibrating in a decaying manner with its damped eigenfrequency. The hydraulic actuators will “feel” these motions and transfer them into the bottom frame. For the experiment the A-20 will be used. During the tests the system is placed unbolts on the factory floor.

During this experiment the input will be a blow with the gangway resulting in a decaying vibration of the gangway. This blow is uncontrollable and unmeasurable. The output will be the system responses. The responses in the bottom frame are measured using the MRUs of the Ampelmann system which are located on the bottom frame. The gathering of the data will be done using CPU's of the Ampelmann system. This makes sure all the signals are synchronized time wise and will automatically convert the data to usable format and is stored.

An overview of the experiment is given in Figure 4-24. During the experiment multiple blows are given with the gangway using a different amount of extension of the gangway and different orientations of the gangway. The lengths of the gangway are gangway completely retracted, gangway halfway extended and fully extended. The first orientation is with the gangway perpendicular to the two MRUs. The second orientation is while the gangway is in line with the two MRUs. For the second orientation due to limited space the test can only be performed with a retracted gangway. This sequence will be performed twice. The first time while the system is in the neutral position, meaning the motion control algorithm is not activated. The second time will be performed while system is actively compensating and the motion control algorithm is activated.

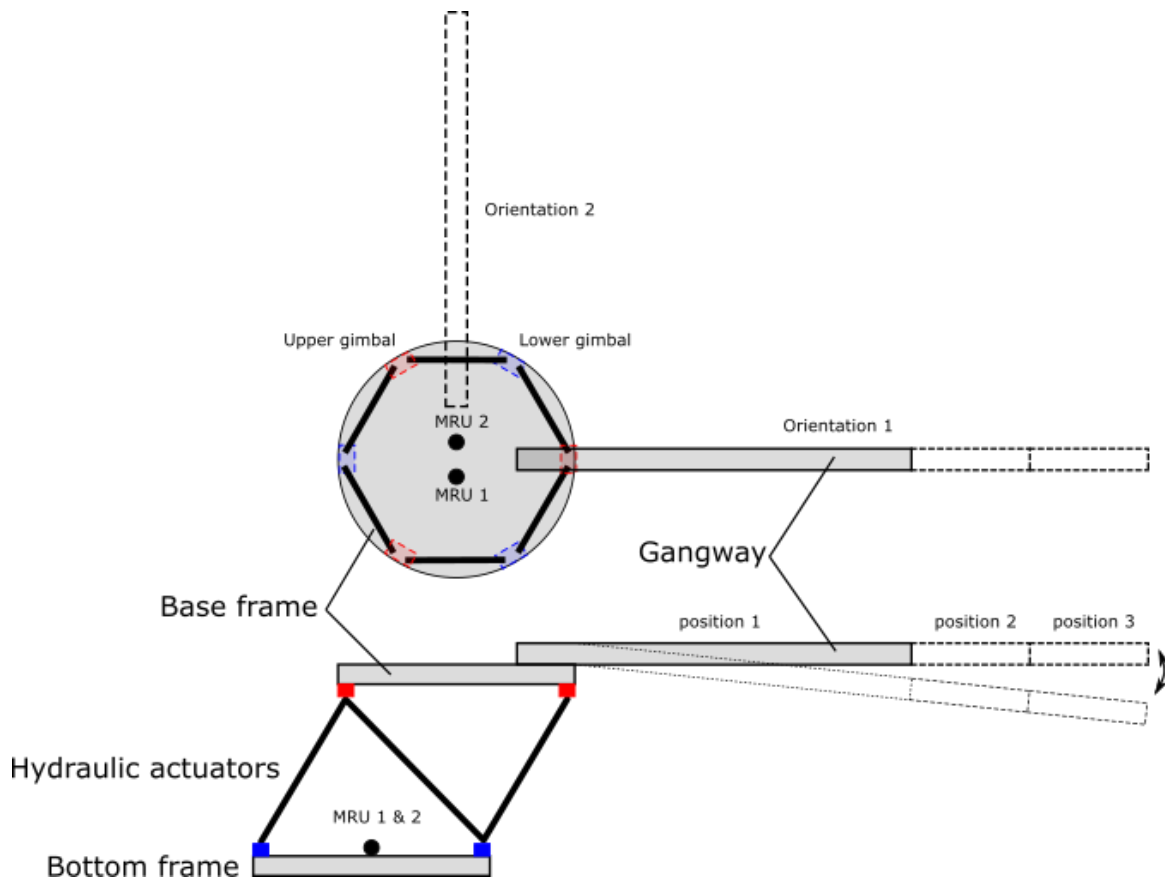


Figure 4-24: Overview experiment vibrations in the bottom frame

Results

In Figure 4-25 the translations and rotations of both the MRUs for the entire sampled time is plotted. In Figure 4-26 the translations and rotations of both the MRUs during a single blow of the gangway is plotted. From the plots the conclusion can be drawn that the gangway is not able to cause vibrations in the bottom frame. For all six degrees of freedom the amplitude of the motions is negligible over the entire test period. Since no responses haven been detected in the bottom frame during this test the conclusion is drawn that what happens on the top of the hexapod cannot cause vibrations in the bottom frame.

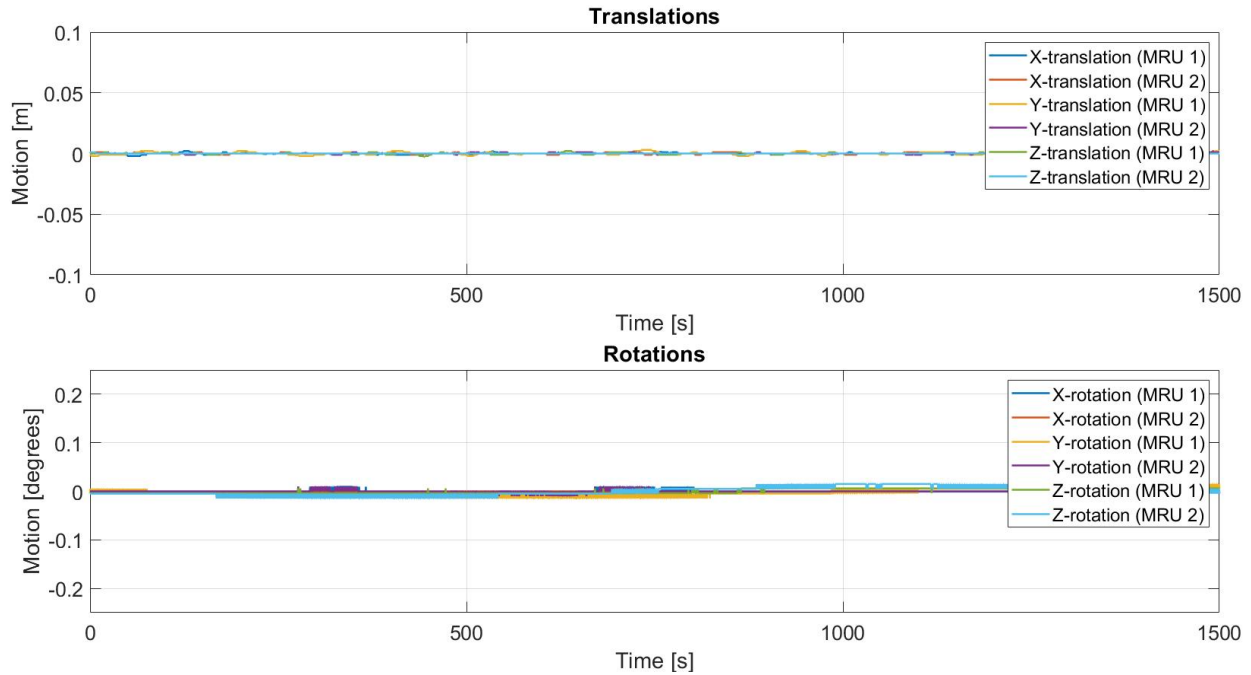


Figure 4-25: A-20 Translations and rotations (entire sampled time)

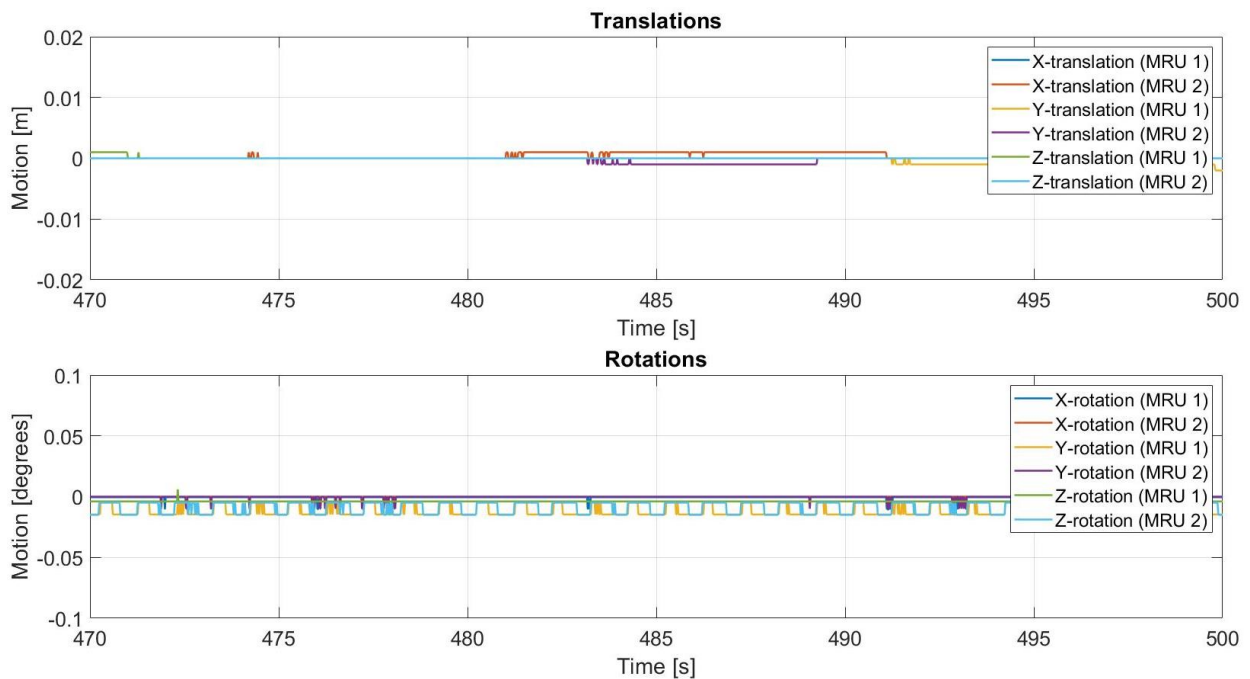


Figure 4-26: A-20 Translations and rotations (sampled time series during single blow with gangway)

4.5 Concluding remarks

To identify possible causes for the unexpected vibrations, measurements are performed on Ampelmann systems. Data which was already available at Ampelmann is analyzed and based on this data three possible causes are determined. These are:

- the influence of the pedestal,
- residual motions due to limitations of the Ampelmann system
- vibrations in the bottom frame due to compensating for gangway motions.

To investigate the influence of the pedestal and the vibrations in the bottom frame two experiments are performed. The residual motions are investigated via calculations based on data readily available.

The result of the experiment, which is performed to investigate the vibrations in the bottom frame due to gangway motions, show that for all six degrees of freedom the amplitude of the response in the bottom frame is negligible over the entire test period. Using these results the conclusion is drawn that the gangway is not able to cause the unexpectedly occurring vibrations. The results from the calculations done to investigate the effect of the residual motions show no amplification concluding that the residual motions do not cause the unwanted behavior.

The experiment to determine the influence of the pedestal shows four peaks in the frequency domain of both the signals. The first is directly caused by vessel motions. The other three have a cause which is not directly related to vessel motions. The data from the sensor on the Ampelmann system, at the top of the pedestal, does not contain a peak which is not present at the ship deck. From this it can be concluded that the eigenfrequencies of the pedestal do not have an influence. For one of these peaks in both of the data sets, namely the fourth peak at 8,1 Hz more energy at the top of the pedestal is present than at the ship deck. At this frequency the pedestal seems to amplify the energy present at the ship deck. A possible explanation for this phenomenon could be the eigenfrequencies and corresponding eigenmodes of the ship deck. The pedestal functions as a lever arm amplifying the rotations related to eigenmodes of the ship deck. This may cause the unexpected vibrations.

5. Analytical model

Ampelmann's motion control algorithm is complicated which makes it difficult to incorporate this algorithm in the FEM model. Because of this there is a need for a second model. This model is a simplified 2D multi-body model. The degrees of freedom will be based on the direction of the most dominant eigenfrequency and corresponding eigenmode determined using the FEM model. Using the simplified multibody model, the equations of motion will be derived where the motion control algorithm will be included. In Figure 5-1 an overview of the desired result is given. The system is represented by three masses: The pedestal + Bottom frame, Top frame and the gangway. The pedestal is assumed to be rigidly connected to the ship deck. At Ampelmann an analytical model (Figure 5-2), made by Temporary Work Design (TWD), is available which will be used as a start.

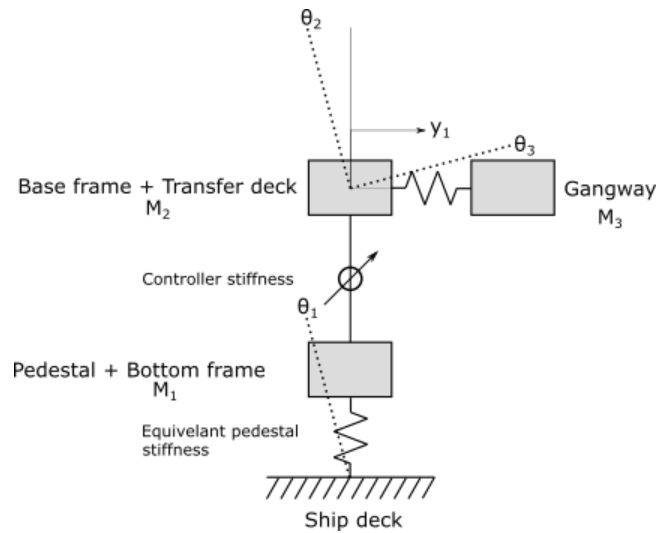


Figure 5-1: Overview of desired result

5.1 Model by Temporary Work Design

Temporary work designs (TWD) has produced a model for Ampelmann (Figure 5-2) [15]. This model is a dual lumped mass model consisting out of two masses which represent the compensated part of the mass and the uncompensated part of the mass of the system. The equations of motion of this model have been determined by TWD and are given in equation 5.1.

$$\begin{aligned}
 I_1 \ddot{\theta}_1 + B_\theta \dot{\theta}_1 + K_\theta \theta_1 &= -F_1 dh + T_1 \\
 I_2 \ddot{\theta}_2 &= -T_1 \\
 M_2 \ddot{y}_2 &= -F_1
 \end{aligned}
 \tag{5.1}$$

F_1 and T_1 represent the actuator forces and the reaction forces between the two masses. However, because the controller of Ampelmann is based on velocity the controller cannot be added in this way. To overcome this a cylinder model is introduced (Figure 5-3). A velocity input is given to the cylinder, which results in velocity input \dot{L}_θ & \dot{L}_y , in other words force is created by moving one end of the spring. The stiffness of the cylinders is assumed to be infinitely high, which means the position of the cart is equal to the position of the compensated mass. The new equations of motion are given in equation 5.2 [15].

$$\begin{aligned}
 I_1 \ddot{\theta}_1 + B_\theta \dot{\theta}_1 + K_\theta \theta_1 &= -F_1 dh + T_1 \\
 \dot{\theta}_2 &= \dot{L}_\theta + \dot{\theta}_1 \\
 \dot{y}_2 &= \dot{L}_y - \dot{\theta}_1 dh \\
 I_2 \ddot{\theta}_2 &= -T_1 \\
 M_2 \dot{y}_2 &= -F_1
 \end{aligned}
 \tag{5.2}$$

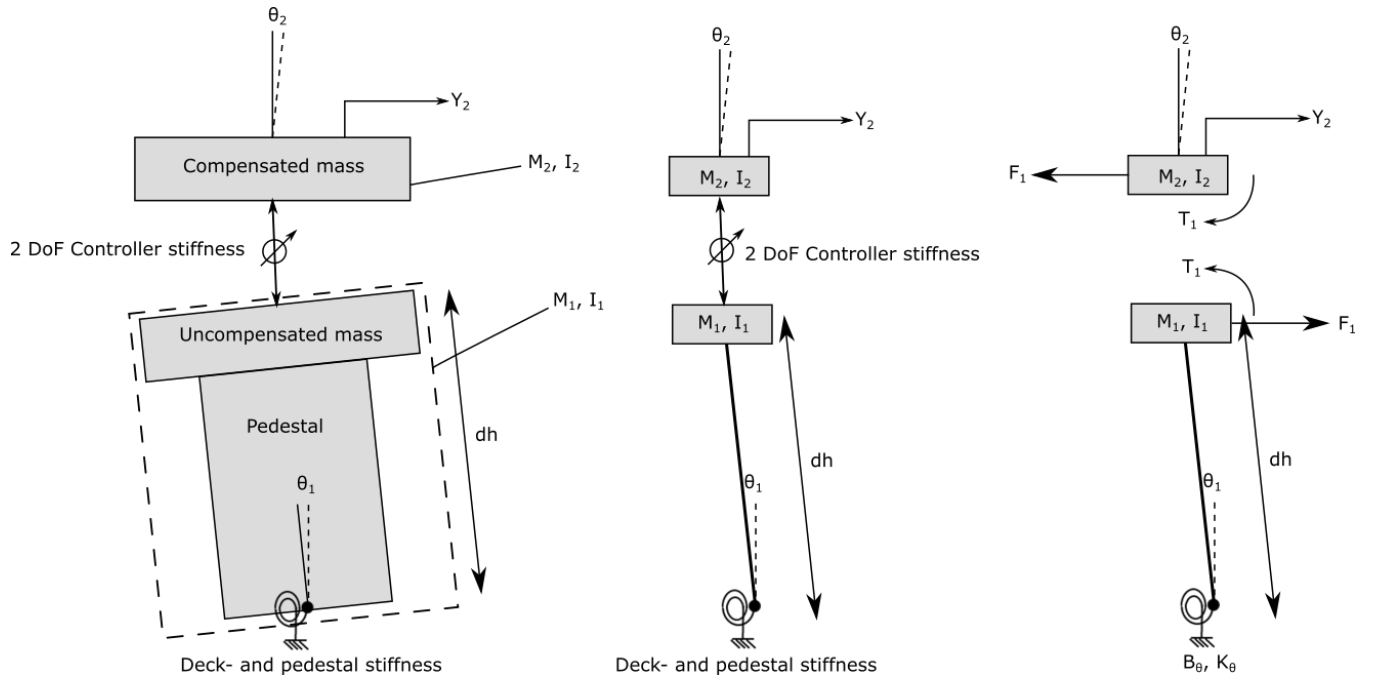


Figure 5-2: TWD model [15]

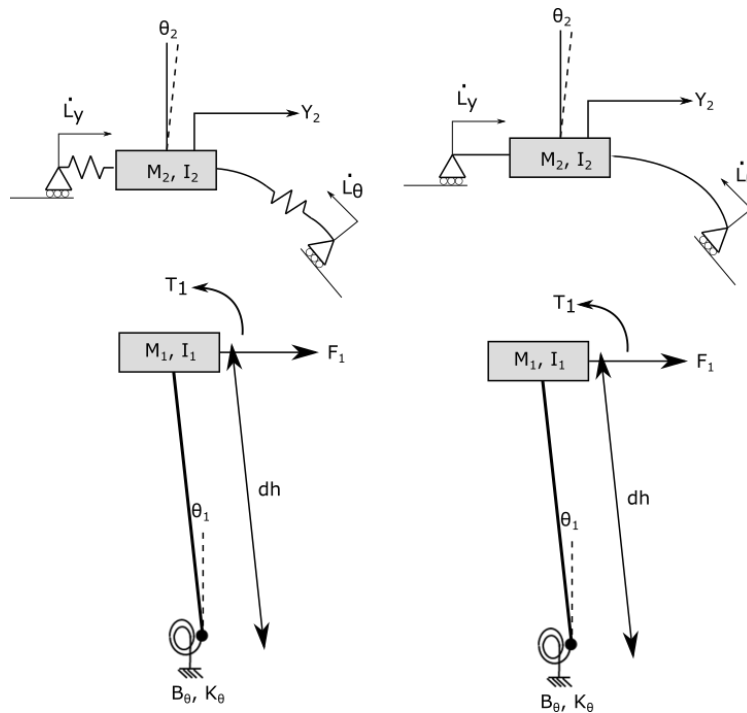


Figure 5-3: Introduction of cylinder model [15]

In Figure 5-4 an overview of the control loop is given. The plant represents the transfer function from cylinder velocity to MRU position. AC represents the actuator dynamics, which in practice means a delay. For more details about the control loop reference is made to [15] & [16]. Using this control loop and the analytical model a state space model is created.

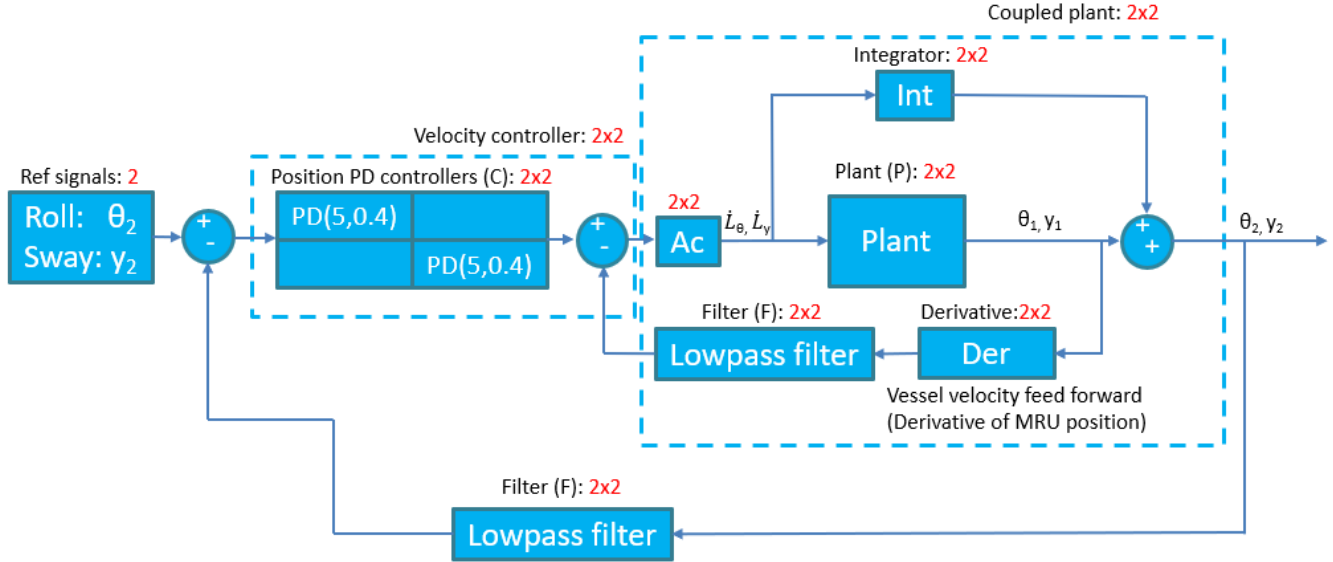


Figure 5-4: Control loop in analytical model

5.2 Differentiation error

As per definition the transfer function is the output divided by the input: $G(s) = y(s)/u(s)$ [17]. In equation 5.3 to 5.6 the transfer functions are worked out.

Laplace transform of equations of motions.

$$\begin{aligned}
 (I_1 s^2 + \beta_\theta s + K_\theta) \theta_1(s) &= -dh F_1(s) + T_1(s) \\
 s \theta_2(s) &= s L_\theta(s) + \theta_1(s) \\
 s Y_2(s) &= s L_y(s) - dh s \theta_1(s) \\
 I_2 s^2 \theta_2(s) &= -T_1(s) \\
 M_2 s^2 Y_2(s) &= -F_1(s)
 \end{aligned} \tag{5.3}$$

Differentiating θ_2 and Y_2 and rewriting.

$$\begin{aligned}
 (I_1 s^2 + \beta_\theta s + K_\theta) \theta_1(s) &= -dh F_1(s) + T_1(s) \\
 I_2 s^2 (L_\theta(s) + \theta_1(s)) &= -T_1(s) \\
 M_2 s^2 (L_y(s) - dh \theta_1(s)) &= -F_1(s)
 \end{aligned} \tag{5.4}$$

Rewriting.

$$\begin{aligned}
 (I_1 s^2 + \beta_\theta s + K_\theta) \theta_1(s) &= dh M_2 s^2 (L_y(s) - dh \theta_1(s)) - I_2 s^2 (L_\theta(s) + \theta_1(s)) \\
 ((I_1 + I_2 + dh^2 M_2) s^2 + \beta_\theta s + K_\theta) \theta_1(s) &= dh M_2 s^2 L_y(s) - I_2 s^2 L_\theta(s)
 \end{aligned} \tag{5.5}$$

$$\begin{aligned}
 P_\theta &= \frac{\theta_1}{\dot{L}_\theta} = \frac{-I_2 s^2}{(I_1 + I_2 + dh^2 M_2) s^2 + \beta_\theta s + K_\theta} \\
 P_y &= \frac{\theta_1}{\dot{L}_y} = \frac{dh M_2 s^2}{(I_1 + I_2 + dh^2 M_2) s^2 + \beta_\theta s + K_\theta}
 \end{aligned}
 \tag{5.6}$$

In the model the second step, the differentiation of the θ_2 and Y_2 , has not been done. In practice this means that instead of the acceleration, the velocity is entered. This results in the transfer functions given in equations 5.7. When the correct transfer functions are used, the real value for one pole and a zero becomes positive (Figure 5-5), indicating an unstable control loop. In appendix F the response of the system is given. This response goes to infinity, as is to be expected with an unstable control loop.

$$\begin{aligned}
 P_\theta &= \frac{\theta_1}{\dot{L}_\theta} = \frac{-I_2 s}{(I_1 + I_2 + dh^2 M_2) s^2 + \beta_\theta s + K_\theta} \\
 P_y &= \frac{\theta_1}{\dot{L}_y} = \frac{dh M_2 s}{(I_1 + I_2 + dh^2 M_2) s^2 + \beta_\theta s + K_\theta}
 \end{aligned}
 \tag{5.7}$$

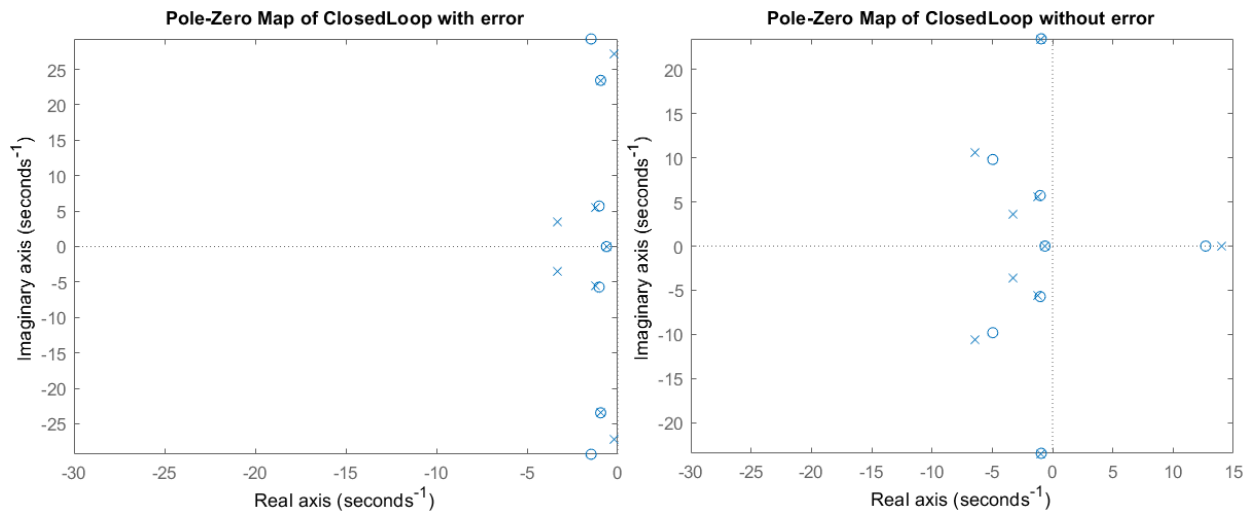


Figure 5-5: Pole-Zero map of closed loop, Left with error & right without error

5.3 Pole plot investigation

In Figure 5-6 the pole plot of the plant and the controller are given. In Figure 5-7 the pole plots of the lowpass feed forward are given. The plots of the plant, controller and the lowpass feed forward all are stable since there are no poles with a positive real value. However, the pole plot of the open loop system does have poles with positive real values and thus is unstable.

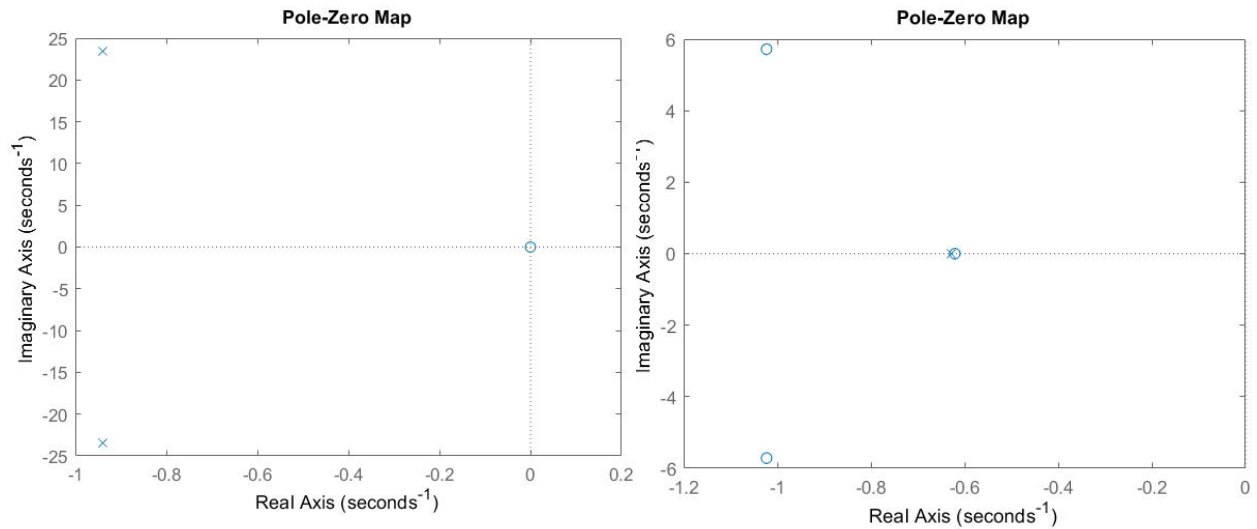


Figure 5-6: Pole zero maps; Left: plant, Right: controller

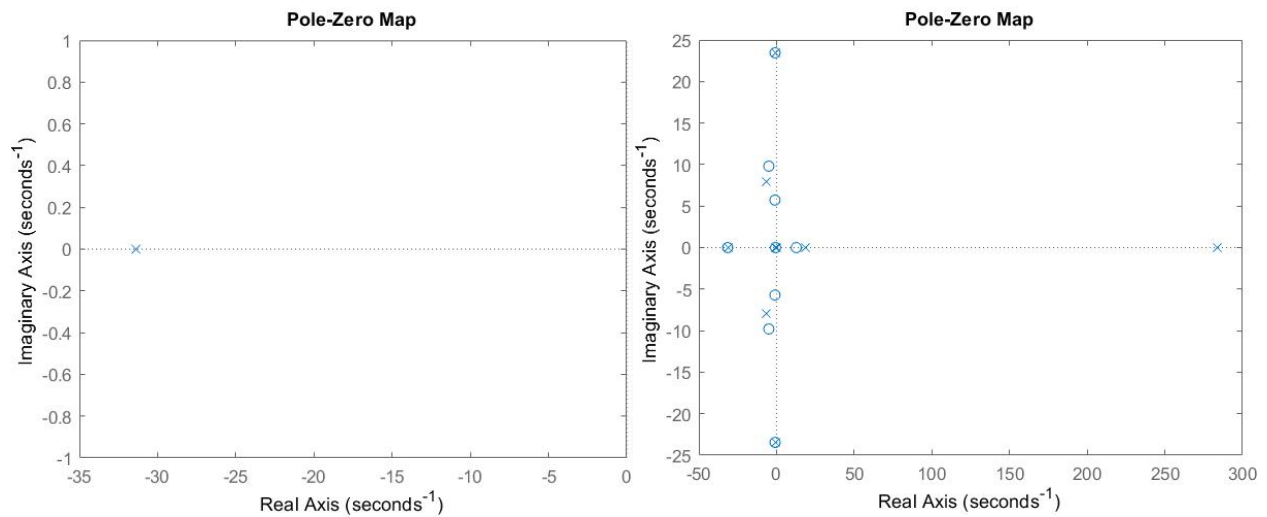


Figure 5-7: Pole zero maps; Left: lowpass filter feed forward, Right: open loop

5.4 Concluding remarks

AmpeImann's motion control algorithm is complicated which makes it difficult to incorporate this algorithm in the FEM model. An attempt is made to create a simplified 2D multi-body model including the algorithm. TWD has produced a model, consisting out of two masses, which should have functioned as the base for this model. During the investigation of the model an error was discovered. The correction of this error resulted in an unstable system. A pole plot investigation is done. However, no explanation for the instability is found.

6. Conclusion and recommendations

6.1 Conclusion

The Ampelmann system occasionally starts vibrating unexpectedly, especially while the system is placed on a pedestal. These vibrations are believed to be caused by the eigenfrequencies of the system and/or amplifications caused by the motion control algorithm. In this thesis an investigation has been done into this phenomenon. A discrete-element model of the Ampelmann system was created to calculate the eigenfrequencies of the system. This model has been created using MATLAB and the toolbox StaBIL 2.0. The first four eigenfrequencies, calculated using the model, are given in Table 6-1.

Table 6-1: Eigenfrequencies A-type and E-type systems

Mode	Eigenfrequency A-type [Hz]	Eigenfrequency E-type [Hz]
1	0.54	0.44
2	2.25	1.73
3	3.19	2.18
4	3.95	2.70

To identify possible causes for the unexpected vibrations data, which was readily available at Ampelmann through the Ampelmann system data network, has been analyzed. Using this, three possible causes have been determined. These causes are: the influence of the pedestal, residual motions due to limitations of the Ampelmann system and vibrations in the bottom frame due to compensating for gangway motions. To investigate these three cases, two sets of experiments and a calculation based on already available data have been done (see paragraph 4.4).

The experiment, which has been performed to investigate the vibrations in the bottom frame due to compensating for gangway motions, shows that the response in the bottom frame is negligible. Using this result, it was concluded that the gangway is not able to cause the unexpectedly occurring vibrations. The results from the calculations done to investigate the effect of the residual motions showed no amplification of energy. From this it was concluded that the residual motions do not cause the unwanted behavior.

The experiment done to investigate the influence of the pedestal shows that amplification of energy at a certain frequency, namely 8,1 Hz, is present. The pedestal could be the cause of the problem. However, instead of "internal" vibrations due to eigenfrequencies (as explained in paragraph 4.3.1), the amplification seems to have a different origin. The pedestal functions as a lever arm amplifying the rotations related to eigenfrequencies and corresponding eigenmodes of the ship deck. This may cause the unexpected vibrations.

An attempt has been made to create a simplified multibody model incorporating the motion control algorithm. This model was supposed to be an extension to a model made by technical work design available at Ampelmann. However, an error in the model has been discovered. The correction of this error caused the model to become unstable. Instead of expanding the model, a pole plot investigation for all the sub parts of the model has been done. However, no explanation for the instability was found.

The objective of this thesis was creating a dynamic model to calculate the eigenfrequencies of the Ampelmann system and explain the unexpectedly occurring vibrations in the Ampelmann system. The eigenfrequencies have been determined using the created MATLAB model. Three possible causes for the unexpectedly occurring vibrations have been investigated. One of these three, the stiffness of the ship deck (paragraph 4.4), was found to be a plausible cause.

6.2 Recommendations

The general consensus at Ampelmann was that the unexpectedly occurring vibrations are caused by eigenfrequencies and corresponding eigenmodes of the pedestal. In this research an indication was found that the origin of the problem is not the pedestal itself, but instead the pedestal functions as an amplifier. Further research is necessary. For example, a desk study could be performed where ship decks, on which the phenomenon occurred, are compared to ship decks on which nothing happened. This research might result in a correlation between deck stiffness and the chance of having the unexpectedly occurring vibrations.

In this research an attempt was made to expand a simplified multibody model of the Ampelmann system. However, the correction of a discovered error in the model resulted in the system having positive real poles, meaning there is an instability in the system. Instead of expanding the model a pole plot investigation is done trying to discover the cause of this real positive pole. The cause of this pole has not been found, so further research is necessary. The model is now based on a linear system of equations. It is recommended to investigate whether these are applicable for the Ampelmann system. The added value of building a relatively simple computer model, in which the motion control algorithm is incorporated, could be quite significant. What could be investigated within this model is:

- How does Ampelmann's algorithm handle vibrations introduced to the base of the system or to the base of the pedestal?
- What is the effect of the height of the pedestal?
- Are there other situations in which the controller becomes unstable?

At the moment Ampelmann is designing the generic A frame, which is a modular pedestal for A-type systems. During the design a lot of research has gone into defining the desired eigenfrequencies of this frame hoping to prevent the unexpectedly occurring vibrations. Based on this thesis, the eigenfrequencies of the pedestal do not play a significant role in preventing these. Instead, the focus should be on the connection between the vessel and the Ampelmann system.

Ampelmann is designing a new gangway system capable of lifting up to 5 tons, where previous systems were capable of lifting up to 1 ton. The different stiffeners in a ship deck of a crane vessel close to a heavy-duty crane are in general much heavier than the general stiffeners below the main deck. These heavier stiffeners are implemented to handle the forces introduced by the crane. To cope with these higher loads of the larger Ampelmann systems, it is recommended that extra reinforcements are added to vessels on which these systems will be installed. It should be noted that these reinforcements are not limited to the main deck but should reach deeper into the ship spanning multiple decks.

In this research in almost all the graphs in the frequency domain peaks are found at 2.3 Hz and 2.6 Hz. The cause of these peaks could not be identified. What could cause these peaks is for example: the internal workings of the sensor or the cabinet of the sensor. Further research into the cause of these peaks is recommended.

7. References

- [1] D. Stewart, "A Platform with Six Degrees of Freedom," *Proceedings of the Institution of Mechanical Engineers*, pp. 371 - 386, 1965.
- [2] K. J. Aström and R. M. Murray, *Feedback systems*, New Jersey: Princeton University Press, 2012.
- [3] A. v. Leer, "Motion Control Enhancements for the Ampelmann System," Master's Thesis, TU Delft, 2012.
- [4] D. Dooms, M. Jansen, G. d. Roeck, G. Degrande, G. Lombaert, M. Schevenels and S. Francois, *Stabil: A Finite Element Toolbox For MATLAB*, Leuven: Katholieke Universiteit Leuven, 2010.
- [5] J. S. Przemieniecki, "Stiffness Properties of Structural Elements," in *Theory of Matrix Structural Analysis*, McGraw-Hill, 1968, pp. 61 - 128.
- [6] T. Yokoyama, "Vibrations of a Hanging Timoshenko Beam Under Gravity," *Journal of Sound and Vibrations*, vol. 141, no. 2, pp. 245-258, 1990.
- [7] H. Feng, Q. Du, Y. Huang and Y. Chi, "Modelling Study on Stiffness Characteristics of Hydraulic Cylinder under Multi-Factors," *Journal of Mechanical Engineers*, vol. 7, no. 8, pp. 447 - 456, 2017.
- [8] A. Bureček, L. Hružík and M. Vašina, "Determination of Undissolved Air Content in Oil by Means of a Compression Method," *Journal of Mechanical Engineering*, vol. 61, no. 7-8, pp. 477-485, 2015.
- [9] Ampelmann, "P18.030.03 AM - E-TYPE GEF XL," Ampelmann, Delft, 2019.
- [10] Y. C. Chung, "Dynamic Analysis of the Ampelmann G25 Gangway," TU Delft, Delft, 2016.
- [11] A. Brandt, "Experimental Frequency Analysis," in *Noise and Vibration analysis: Signal Analysis and Experimental Procedures*, Wiley, 2013, pp. 207-250.
- [12] A. Brandt, "Spectrum and Correlation Estimates Using the DFT," in *Noise and Vibration Analysis: Signal Analysis and Experimental Procedures*, Wiley, 2011, pp. 251-295.
- [13] D. Jakobovic, "Forward Kinematics of a Steward Platform Mechanism," Faculty of Electrical Engineering and Computing; University of Zagreb, Zagreb, 2002.
- [14] F. N. Catbas, T. Kijewski-Correa and A. E. Aktan, *Structural Identification of Constructed Systems Approaches, Methods and Technologies for Effective Practice of Structural Identification*, Reston: American Society of Civil Engineers, 2013.
- [15] Temporary Work Design, *Frequency analysis*, Delft: TWD, 2019.
- [16] Temporary Work Design, "TWD NL 2019 030C 100 REV 0 Dynamic model of A-type Ampelmann with pedestal-TF," TWD, Delft, 2019.
- [17] S. Skogestad and I. Postlethwaite, "Multivariable Feedback Control Analysis and Design," Wiley, 2007.

- [18] J. N. Reddy, Introduction to Nonlinear Finite Element Analysis, New York: Oxford University Press, 2004.
- [19] B. Friedland, CONTROL SYSTEM DESIGN An Introduction to State-Space Method, New York: Dover Publications, 2005.

8. Appendix

A. Standard block diagram elements

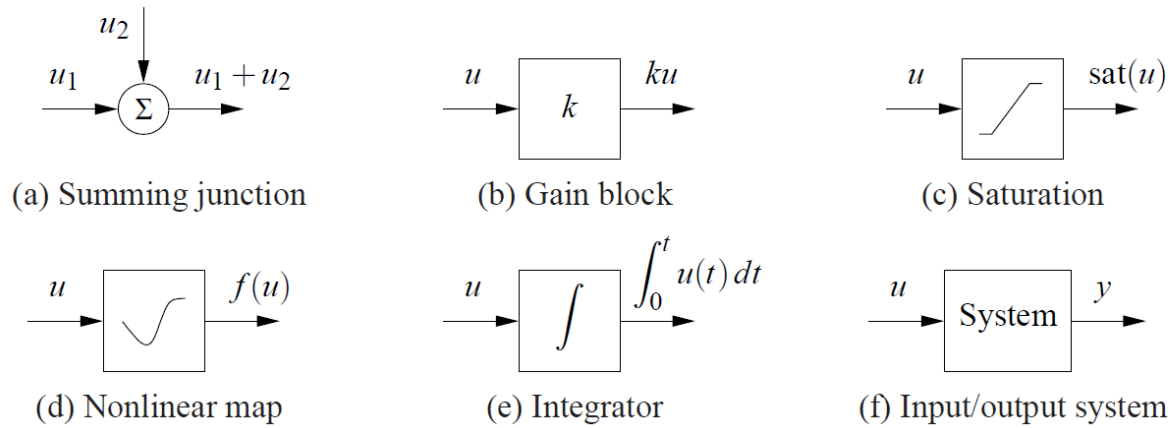


Figure 8-1: Standard block diagram elements [2]

C. Time domain A-28, A-29, E-04 & E-14

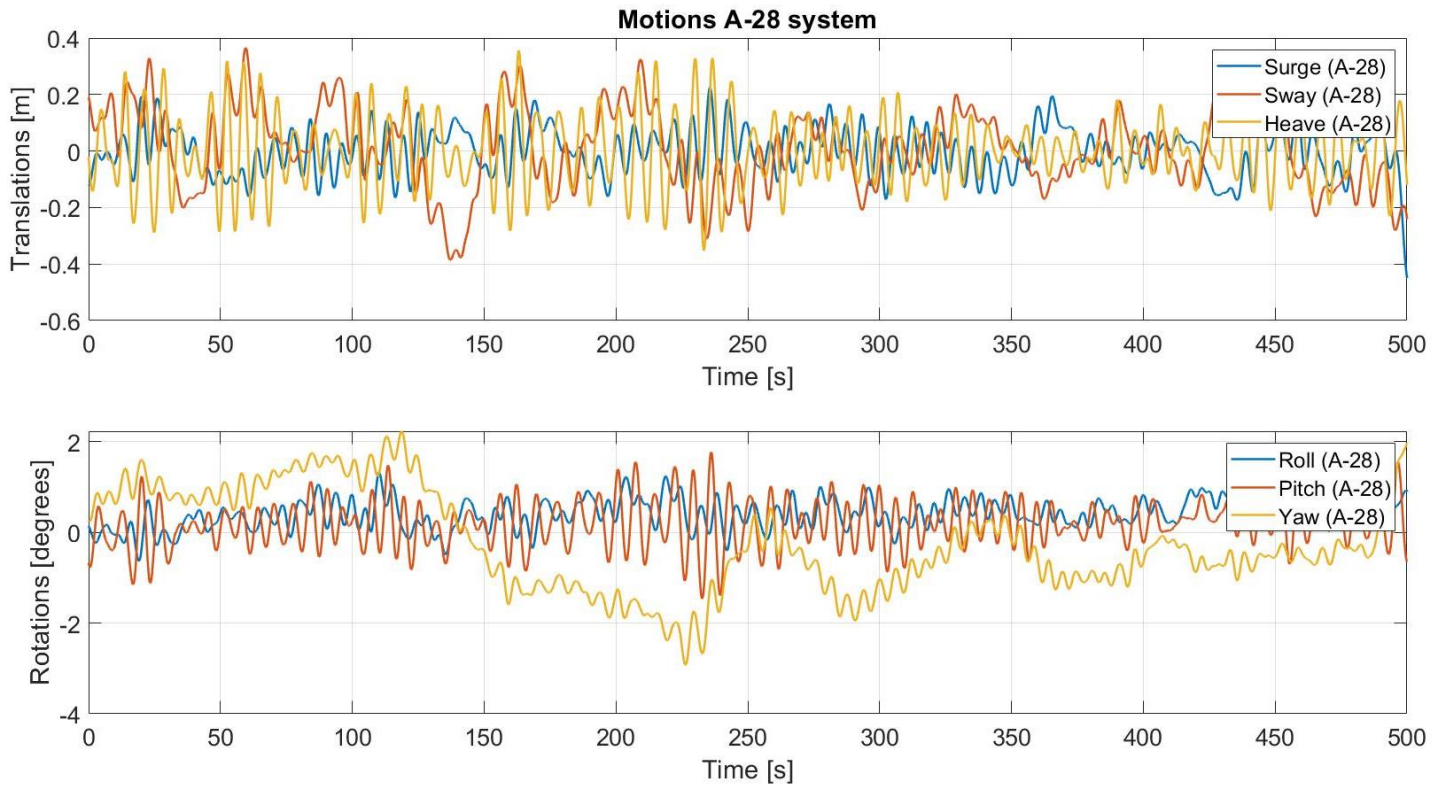


Figure 8-2: Time domain A-28 system

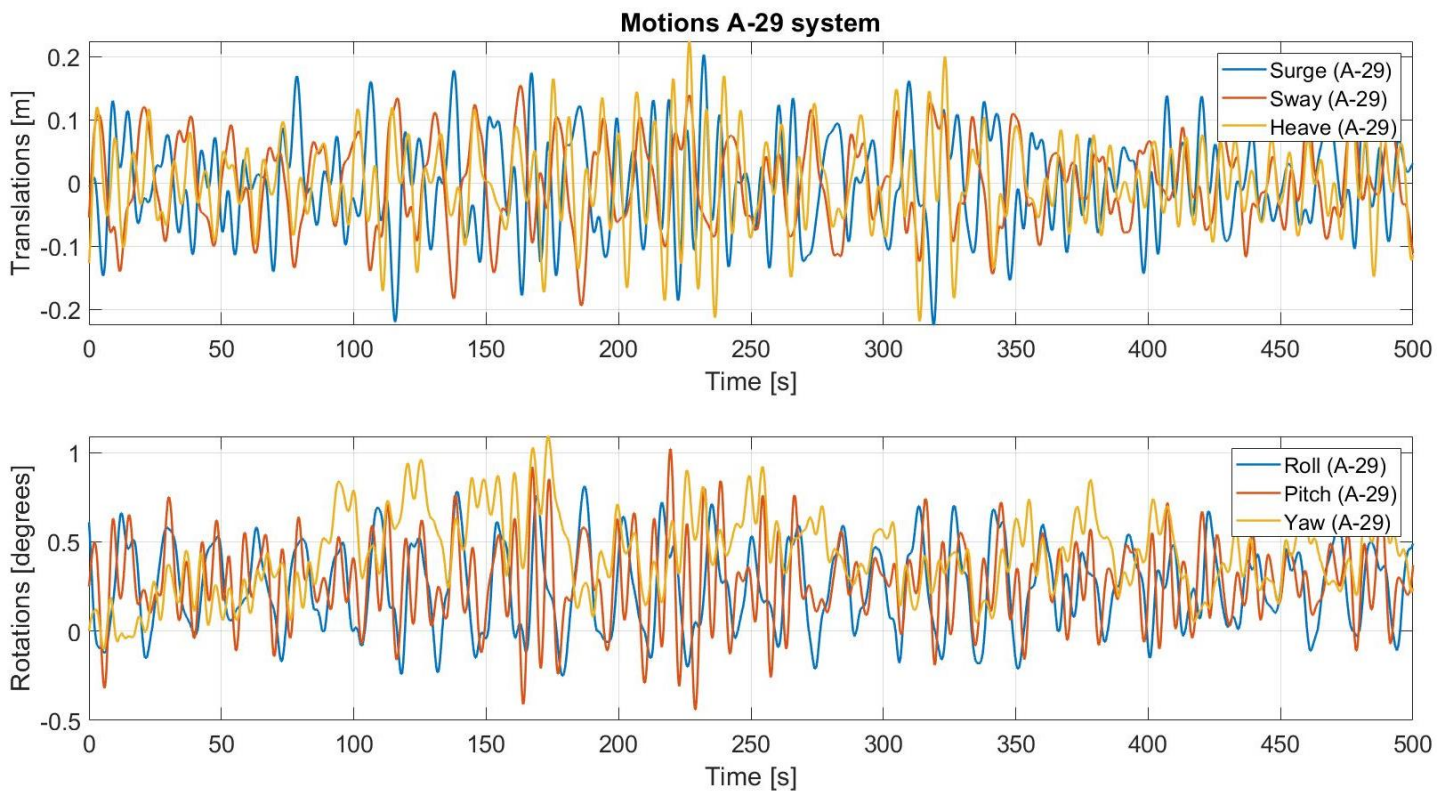


Figure 8-3: Time domain A-29 system

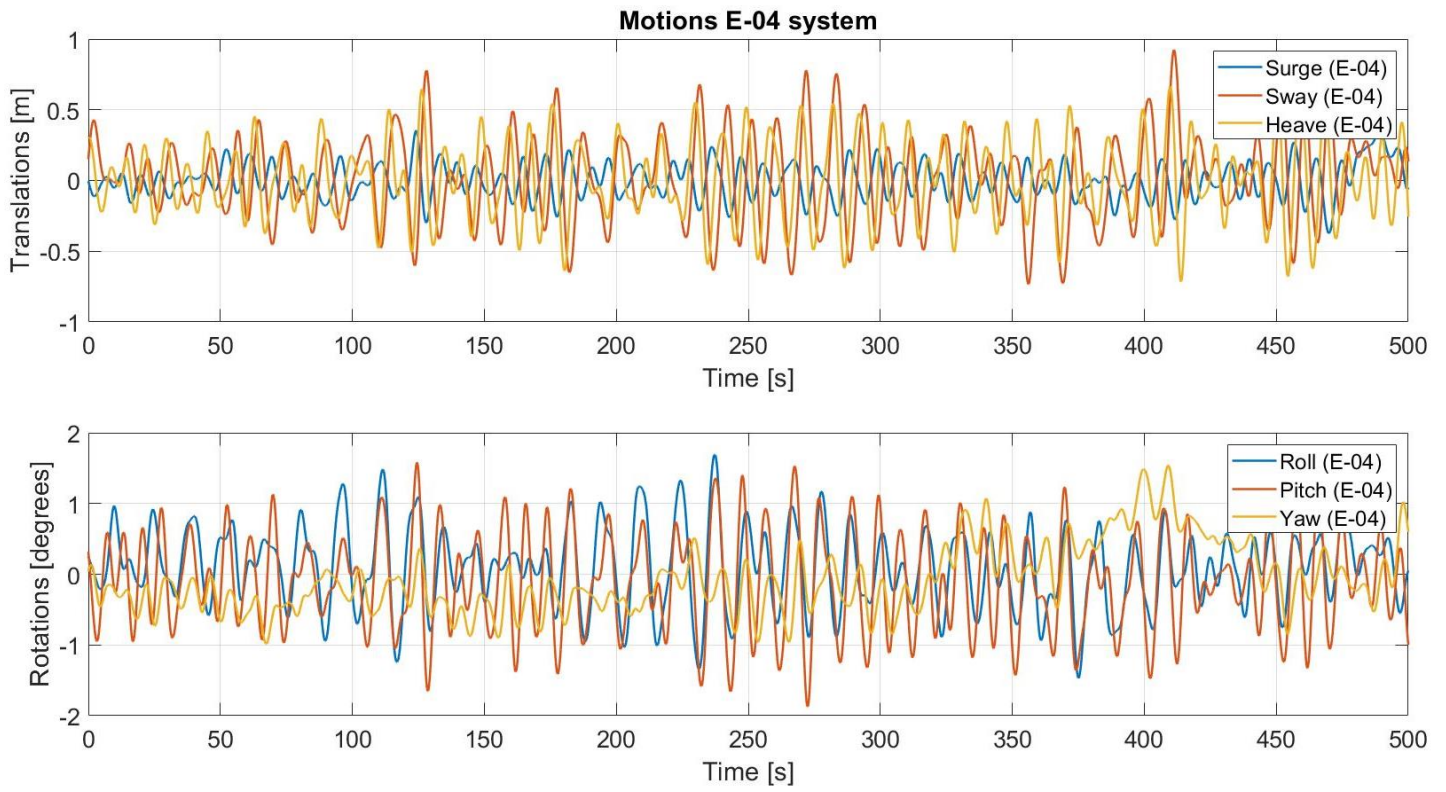


Figure 8-4: Time domain E-04 system

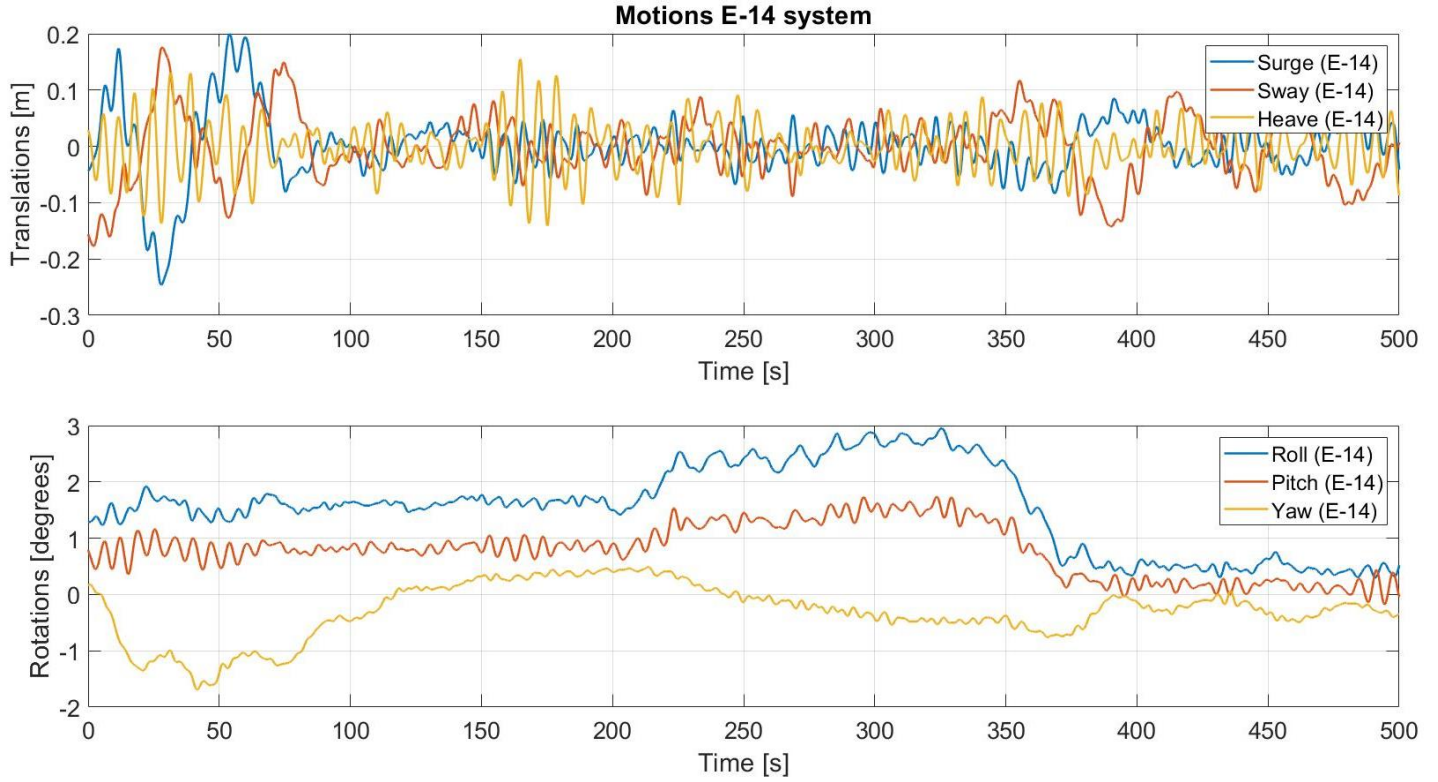


Figure 8-5: Time domain E-14 system

D. Vessels on which the different systems are installed

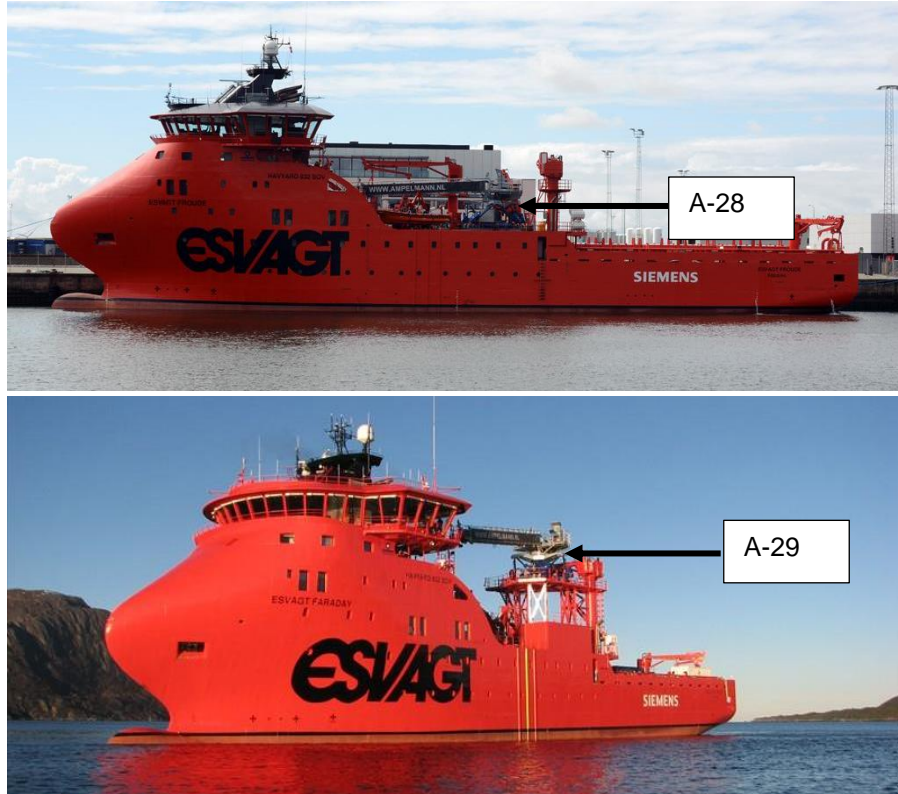


Figure 8-6: A-28 without pedestal (upper), A-29 with pedestal (lower)

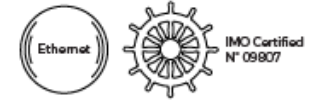


Figure 8-7: E-04 on pedestal (upper), Olympic Orion, no picture with Ampelmann system available (lower)

E. MRU (Octans) specifications

Octans

Technical specifications



Performance

Heading Accuracy ⁽¹⁾⁽²⁾⁽⁴⁾	0.1° seclat (Autonomous)/0.05° seclat (with GPS input)
Settling time (typical)	5mn
Resolution	0.01 deg
Heave/Surge/Sway Accuracy	5cm or 5% (whichever is greater)
Delay Heave/Surge/Sway Accuracy	2.5cm or 2.5% (whichever is greater)
Heave periods	up to 30sec
Roll/Pitch/Yaw Dynamic accuracy ⁽²⁾	0.01 deg
Resolution	0.001 deg

Operating range/environnement

Rotation rate dynamic range	Up to 750 deg/s
Acceleration dynamic range	±15 g
MTBF	100,000 hours
Operating/storage temperature	-20 °C to +55 °C/-40 °C to +80 °C
Heading/roll/pitch	0 to +360 deg/±180 deg/±90 deg
Shock and vibration proof	

Physical characteristics

Dimensions (L x W x H)	275 x 136 x 150mm
Weight In air	4.5kg
Water proof	IP66 & IPx7
Material	Aluminum
Same footprint & dimensions as 4 th generation OCTANS	

Interfaces

User Interface	Web-based Graphical User Interface
Serial RS232/RS422 port	3 outputs/2 Inputs/1 configuration port
Ethernet port ⁽⁵⁾	5 outputs/4 Inputs flow: UDP/TCP Client/TCP server
Pulse port	PPS Input for < 100µs time synchronization
Input/Output formats	Industry standards: NMEA0183, ASCII, BINARY
Data output rate	0.1Hz to 200Hz real measurements
Timing	Fix latency 2.35ms, < 200µs Jitter
Power supply	24 VDC
Power consumption ⁽⁶⁾	18W
Same connectors and protocols as previous generation Octans	

Figure 8-8: MRU (Octans) specifications

F. Octans & ship to ship data E-04 (difference)

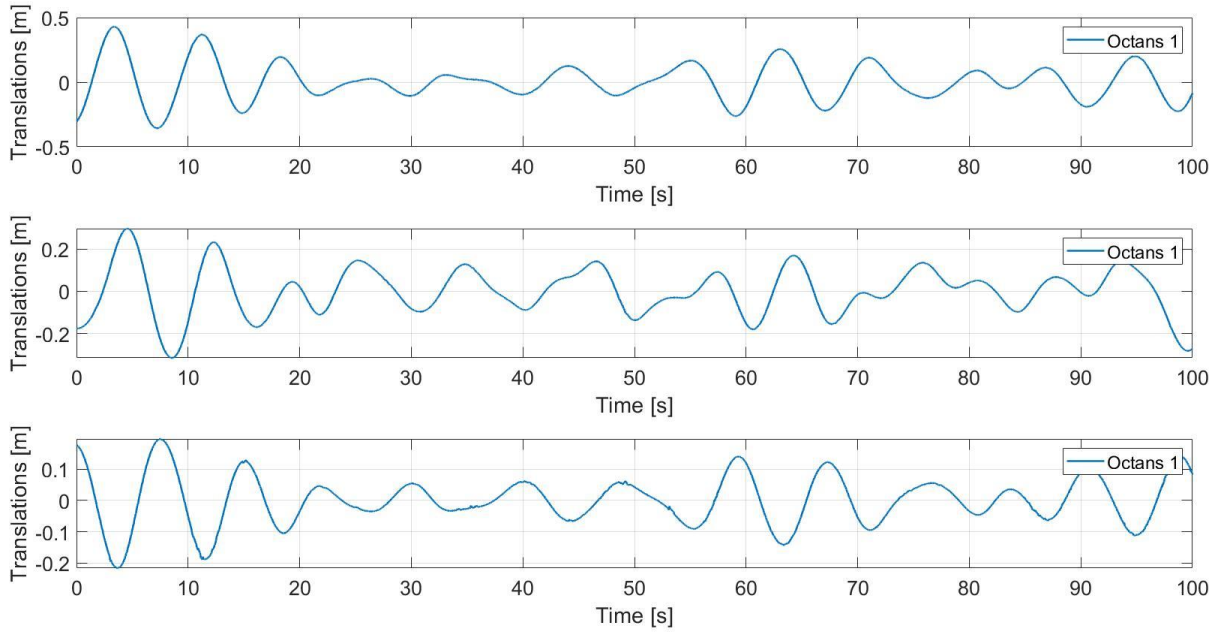


Figure 8-9: E-04 Translations difference (time domain)

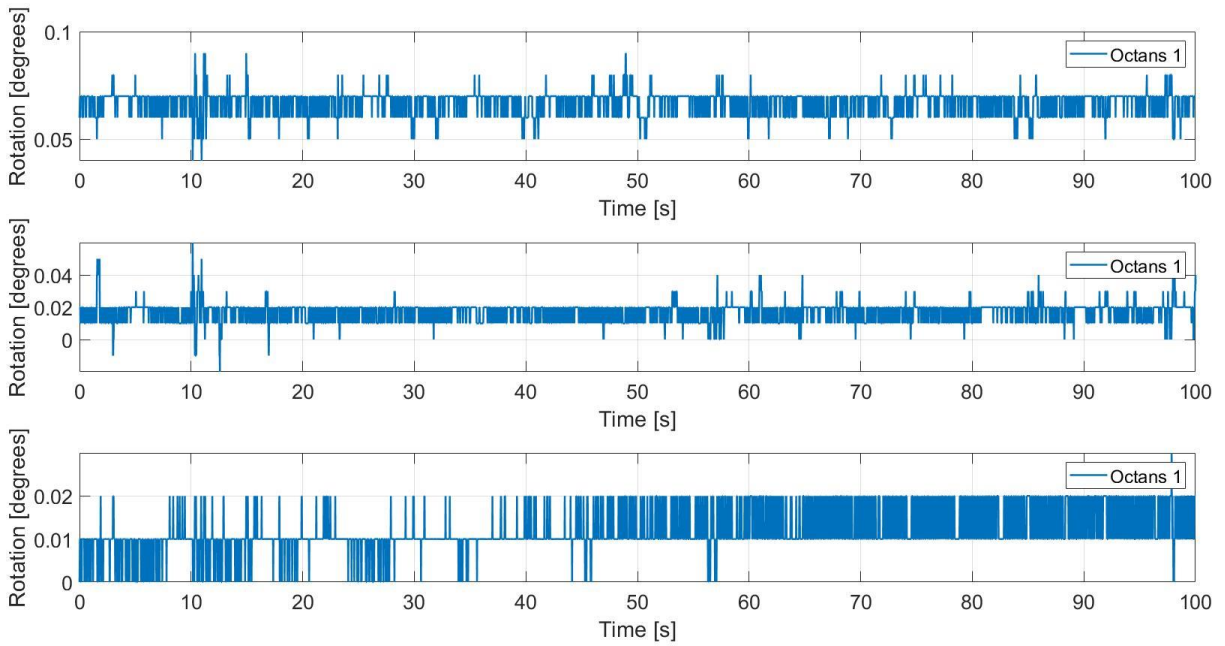


Figure 8-10: E-04 Rotations difference (time domain)

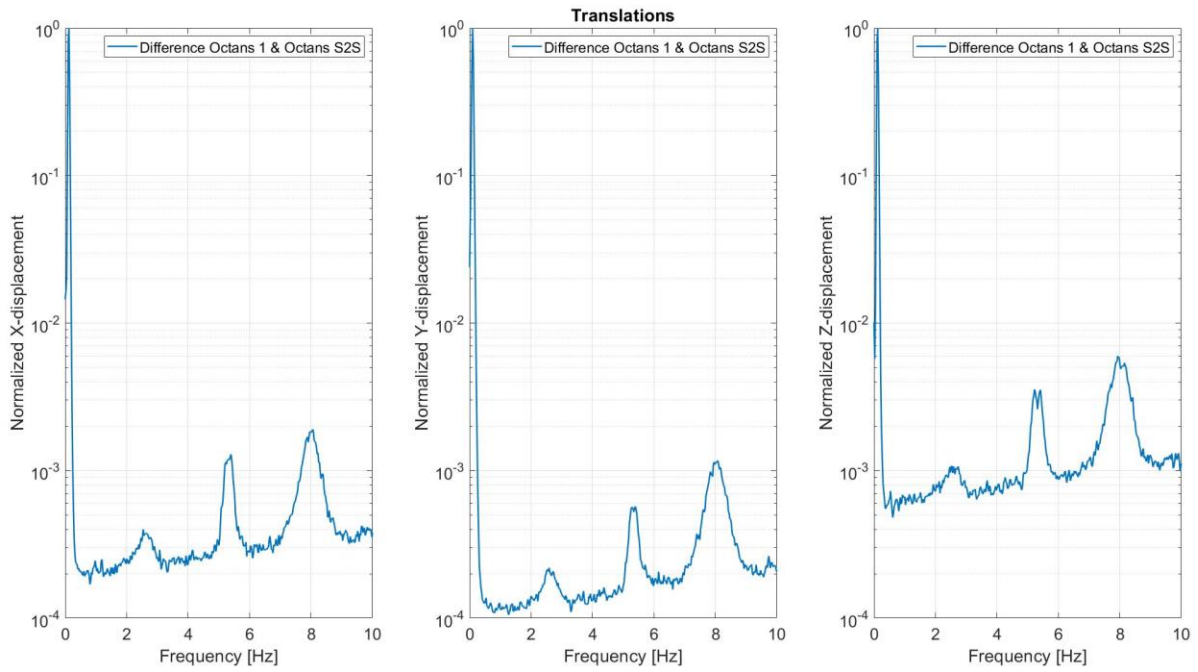


Figure 8-11: E-04 translations difference (frequency domain)

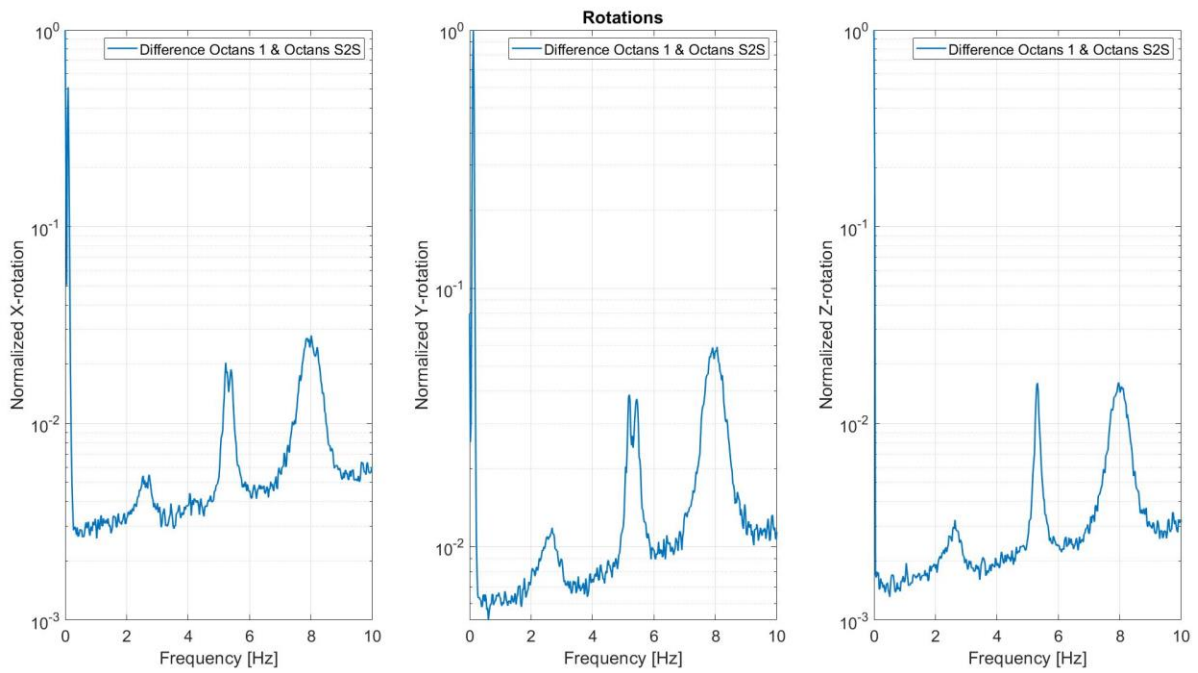


Figure 8-12: E-04 Rotations difference (frequency domain)

G. Excitation analytical model

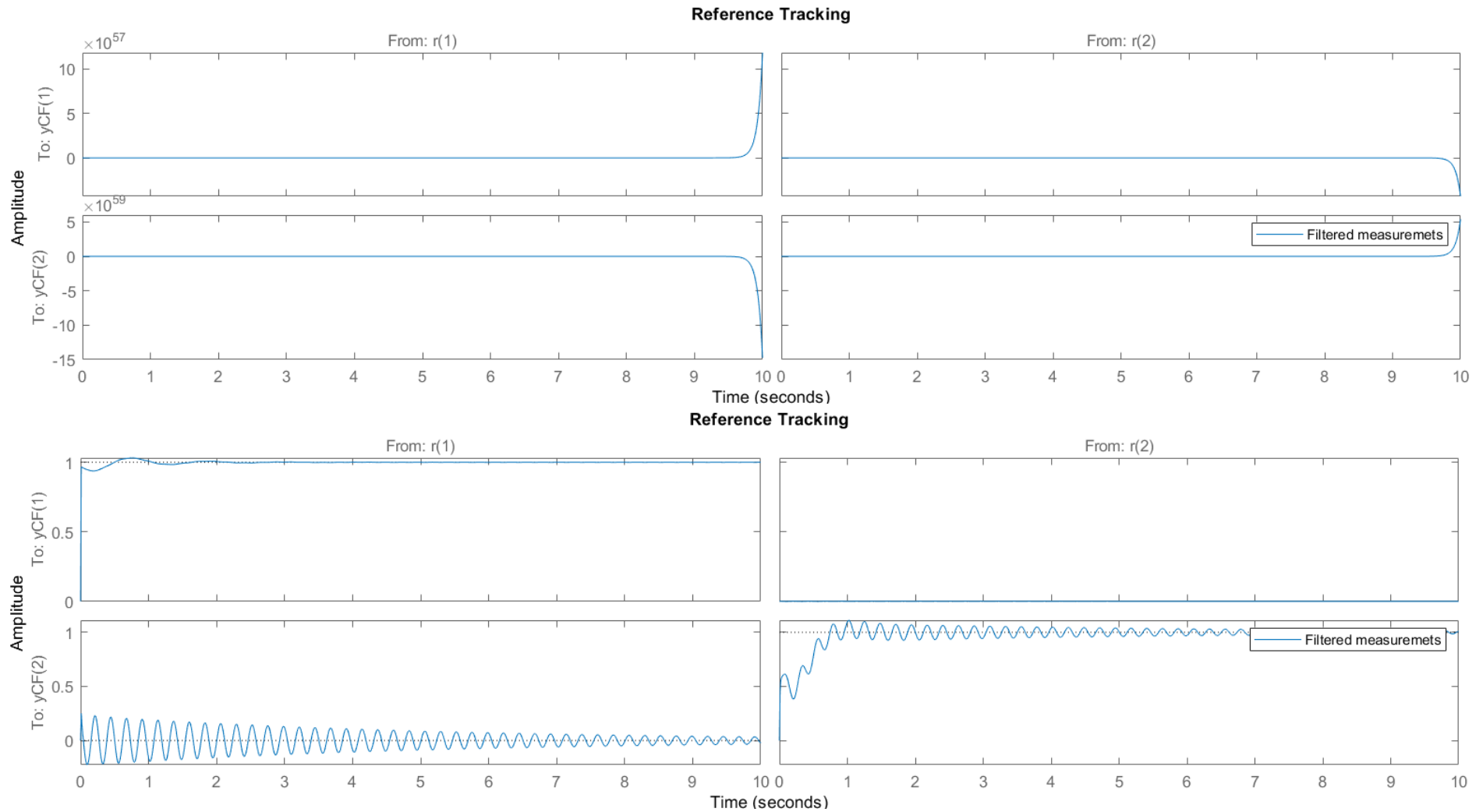


Figure 8-13: Response analytical model

